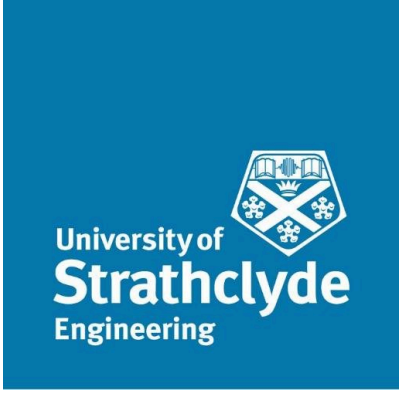

Mechanical & Aerospace Engineering Department

SAFE COMPOSITE BIKE HANDLEBAR

Authors:

JOSÉ JAIME FERNÁNDEZ ÁLVAREZ

CÉSAR MARTÍNEZ FERNÁNDEZ

JOSÉ LUIS VIÑAS SALGADO

MATTHEW NOBLE

Supervisor:

DR. MEISAM JALALVAND

Mechanical Engineering

Group Project

Final Report

Abstract

Tests on CF tubes were carried out with the purpose of getting a good understanding about how CF performs under load until its failure. It could be seen that in all the samples the break was catastrophic and that no warning, nor visual or acoustic, warned of the immediate snap. These results were used later on to simulate and then manufacture a layup around the tube that will fail before and in a gradual mode. This will cause a gradual failure of the whole tube and it is used as a warning of the snap that will come immediately. Finally, the reinforced tubes with the layups were tested and the results were compared with the ones obtained in the naked tubes.

Table of Contents

Figures Index

Tables Index

1. Introduction

A bicycle handlebar is the steering control for bicycles. It also often supports a portion of the rider's weight, depending on their position, and provides a mounting place for brake levers and gear shifters [1]. Aluminium and carbon fibre (CF) slowly started to be used as the principal material for high performance bicycle frames and handlebars towards the end of the 20th century. The development of expensive mountain and racing bicycles has led to CF and aluminium becoming the most common materials when talking about high performance bike handlebars.

Aluminium has good mechanical properties. It is comparatively lighter than other metals such as steel, and is cheaper than CF. Another characteristic of aluminium is that when it is damaged, a noticeable plastic deformation before total failure warns the cyclist that it is time to replace the part. These advantages make aluminium handlebars an attractive option for cycling enthusiasts and leading companies. On the other hand, CF is more expensive, but it is even lighter than aluminium due to its lower density. Most handlebar brands show a weight saving of around 20 – 40 per cent for CF over aluminium [2].

In handlebar applications at the same weight, CF offers 2 to 5 times more stiffness than aluminium and steel. In the same way strength is higher in CF [3]. Another important advantage of using this material on bicycle handlebars is that more complex geometries can be manufactured with sleeker designs resulting in a more aerodynamic part [2].

However, there is a negative aspect derived from the use of this material: when a CF handlebar snaps, it does so suddenly, without warning, due to the non-ductile behaviour of the material. This sudden catastrophic failure by un-warned snapping of the component is highly dangerous and has resulted in life changing consequences to the victims of such failures. As throughout engineering in the 21st century safety is the most important characteristic in all designs, and this is where CF handlebars fall short. The characteristics of these two materials are summed up in the following table.

Table 1: Pros and cons of materials in handlebars

Material	Pros	Cons
Aluminium	Cheaper, gradual failure (plastic deformation)	Heavier, limited geometries
CF	Lighter, more complex geometries, stiffer, stronger	More expensive, catastrophic snap

2. Project Scope

2.1. Aim

The aim of this project is to increase the safety of bicycle handlebars by applying a layup made from different composite materials that, through its failure, warns when the catastrophic snap is about to occur.

2.2. Methodology

In this context a CF tube similar in geometry to a bicycle handlebar is used as a simplified model for this work. The project was divided in the following four parts:

- Part 1: Initial tests.

First of all, the CF tube was tested on a bending test machine to understand how it performs when it is under load and how much strain and stress it is able to withstand before failure.

- Part 2: Simulation with FEA.

Using the data obtained in the previous part, an accurate representation of the tube was modelled. Then, the hybrid layup was designed around it.

- Part 3: Manufacturing.

Once the layup is designed in terms of materials, dimensions and configuration, it is manufactured and applied to the tube.

- Part 4: Final tests.

Finally, the upgraded tube was tested to analyse the expected gradual failure, comparing these results with the ones obtained in the initial tests.

3. Project Management

For this project, each of the team members had to do an intense research of information about bike handlebars, composite materials, how these are manufactured and what their properties are.

The way in which the group decided to tackle the project influenced how the group worked. We had specific jobs within the group in order to get the most out of the four of us. The aim was to have all members become specialists towards a certain aspect of the project.

All the aspects involved in the bending tests were addressed by Luis and César. César, more specifically, designed the different parts needed for the tests and applied the measuring systems on the CF tubes, whereas Luis, using a specific software, collected and processed the data obtained.

The modelling and FE analysis on the bar using ANSYS software was explored by Jaime. The design of the layups was performed by him as well. Matthew, after looking up into possible layup materials and the available manufacturing techniques, was the one to put the reinforced handlebar together by applying the designed layup.

In addition, Matthew was the person responsible for the external communication, making a link between the group, the supervisor and other entities. Luis also documents the meetings of the group with the supervisor, to have a better control of our progress, addressing the different issues that are discussed in them.

Media creation was made by César, who took pictures, and Luis, who recorded video clips of each stage of the project. The web page was done by both César and Jaime. Useful papers, media and general progress of the work were posted to our Google Drive group, so easy access to those tools is guaranteed to every member.

Regarding the communication plan, we met weekly. Further contact was made through WhatsApp, where meeting schedules were set, and different aspects of the work discussed. At the end of each weekly meeting, updated work or aims for each person were given for the following week. Fortnightly meetings with the advisor were arranged via email. In them, we updated our advisor on what we had done, commented about certain concerns and asked for insight related to the achieved results of each part of the work.

A Gantt chart was initially created to base our schedule onto it, giving an idea of when certain tasks needed to be finished. The Gantt chart was updated as progress was done due to a more in-depth understanding of the work and its related timings. As

with most projects, some issues had to be faced, which influenced the overall planning. Delays in the manufacturing order of the parts for the tests and the shipping of the materials, limitations in the accessibility of the tools provided in the lab contributed to this matter.

Acknowledging the overlapping way of assigning the different tasks of this work, a summary of the division of the work is shown in Table 2

Table 2: Project management

Task	Member
Bending tests	Luis and César
Simulation	Jaime
Manufacturing	Matthew and Jaime
Media	Luis and César
Communication and Manager of the group	Matthew

4. Technical Progress

4.1. Initial tests

Handlebars, by the simple act of riding, are subjected to variable flexural loadings. In this scenario, fatigue testing could be a sensible option to address but, as polymer-based epoxy CF handlebars have in most cases a very long lifespan in fatigue [1], this approach was discarded.

Another common testing method in the industry is the impact test, where weights are fixed in the ends of the handlebar, and it is dropped from certain height to analyse how it behaves. As useful as the information this method brings when talking about impact behaviour, it could not provide an accurate representation of the failure point, compared to the quasi-static approach in a bending test. It is this slow progress that enables the monitoring of the different parameters of interest. The easy access to flexural machines and rigs in the labs, and the simpler and arguable safer process made this last method the chosen one for the project.

In a three-point bending test, the fibres on the top are under compression, and the fibres on the bottom under tension. As a first impression, it is assumed that the CF tube will break on the compressive side, as CF under compression performs, in general, worse than in tensile loading because of its internal configuration. This is explained by a process called micro-buckling [], where the fibres debond from the matrix (due to compressive elastic or plastic deformations) and buckle.

Three forces are experienced by the handlebar: two downward applied by the rider's hands and the upward reaction produced by the stem (part of the bicycle that connects the handlebar and the frame). Figure 1 describes this scenario, being F an arbitrary force.

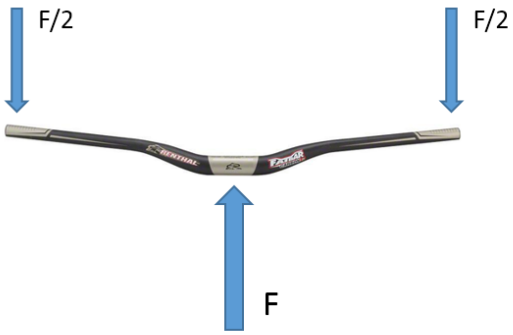

Figure 1: Forces representation in a handlebar

This loading state was recreated on the test as follows in Figure 2. The two systems are equivalent but with the forces in opposite directions. The machine applies the force downwards in the middle of the tube, while the side supports provide the reaction forces.

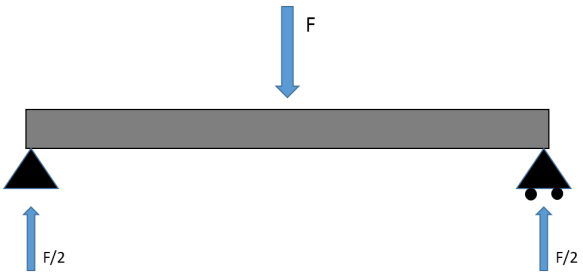

Figure 2: Forces representation in a bending test

A bending test diagram is shown in Figure 3**,** which represents the shear forces, bending moments and bending deflection through the length of the specimen.

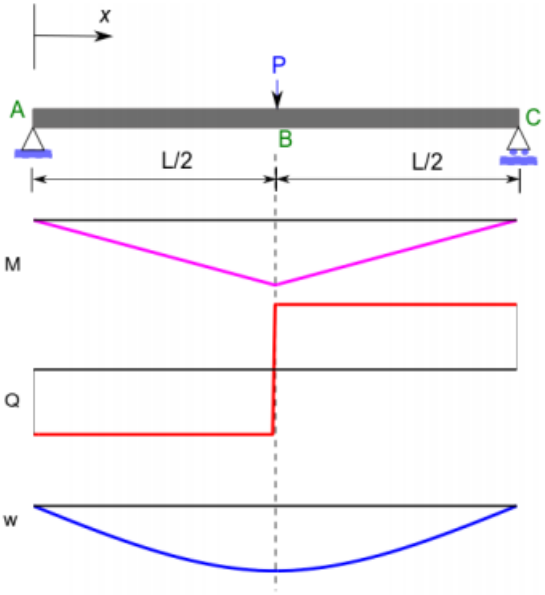

Figure 3: Bending test analytical solution

In this project three tests were carried out on three CF tubes that shared the same geometry and properties. These tests were carried out on three tubes configured with a constant displacement of the loading nose, and force values were acquired for each time step. The distance between supports was set to 450mm, determined by the tube dimensions.

4.1.1. The CF tubes.

The tubes subject to test were roll-wrapped, made from a 2D woven fabric with a matte surface finish. The dimensions are shown in the Table 3**.**

Table 3: CF tube data

Length (L)	500 mm
Outer diameter (OD)	30 mm
Inner diameter (ID)	28 mm
Thickness (T)	1 mm
Type of fibres	Woven

An important parameter taken into account in order to avoid shear failure was the aspect ratio between the span of the supports (L_{span}) and the outer diameter of the tube. An aspect ratio greater than 10 is desirable for this purpose [2], the closer to 20 the better.

For the tube selected, the aspect ratio was:

$$r = {L_{span}}/{OD} = {450}/{30} = 15 > 10$$

A way to increase the aspect ratio is by extending the distance between the supports, which in this case was not possible due to the length of the tube, which was set to 500 mm due to availability issues. Reducing the diameter of the tube could also help get a greater aspect ratio but maintaining a relatively large outer diameter was thought to be a necessary compromise, as it would facilitate the application of the layup in the manufacturing stage of the project. Nonetheless, the general proportions of commercial handlebars were respected, so reasonable values could be achieved.

4.1.2. Boundary conditions.

To obtain a flexural behaviour, the tube had to be constrained in a certain manner. Attending the configuration shown in Figure 3, rotation must be allowed on both ends of the CF tube. While one side should be constrained for the X displacement and the other free, the use of rubber allowed in equal parts to have a proper grip to

prevent the bar from slipping from the desired position and, at the same time, allowed for some movement related to the deformation of the tube.

The design of the supports and loading nose constitute a physical representation of the boundary conditions of the tests. Both supports and, most importantly, the loading nose, show a half cylindrical feature to increase the surface area in contact with the carbon tube. The inner radius of the cylindrical parts is 17 mm, to let it accommodate a 2 mm thick rubber sheet between them and the CF tube. This could achieve smaller stress concentrations in the tube at the loading and support regions, preventing it from crushing.

Figure 2 shows the loading nose, which has a rectangular-based prism welded to the cylindrical part, to let the fixture of the test machine clamp to it securely. The length of it is 100 mm as it presses onto the region of the bar that withstands more loading force (See Appendix I for detailed drawings).

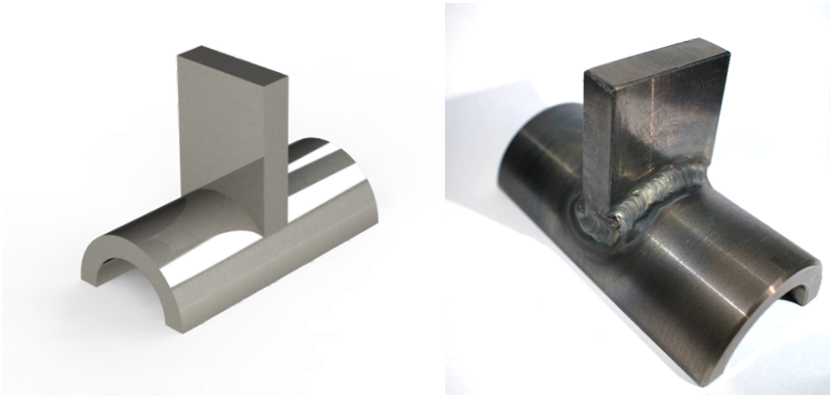

Figure 4: Nose support designed and manufactured

The lateral supports have a variable-section rod, threaded on both ends, that helps centre the tube easily on the rig. Around this rod the part rotates to accompany the movement of the ends of the CF tube when it bends.

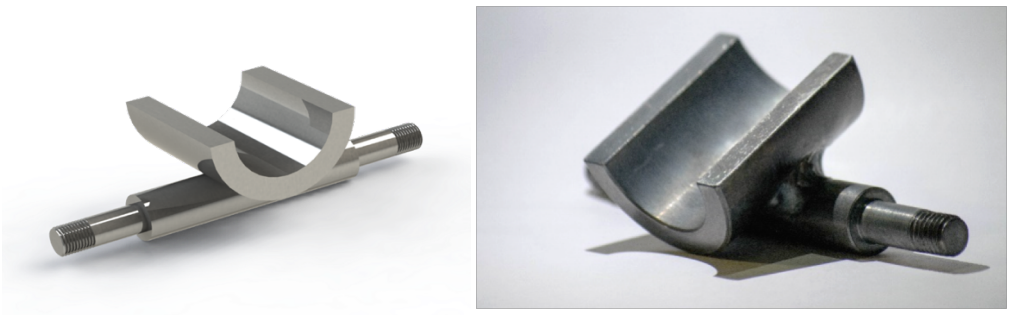

Figure 5: Support designed and manufactured

The design of the previously mentioned parts were subject to the dimensions of the rest, shown in the Figure 4, as they were already manufactured. The dimensions of the tube played a role in the design of the supports.

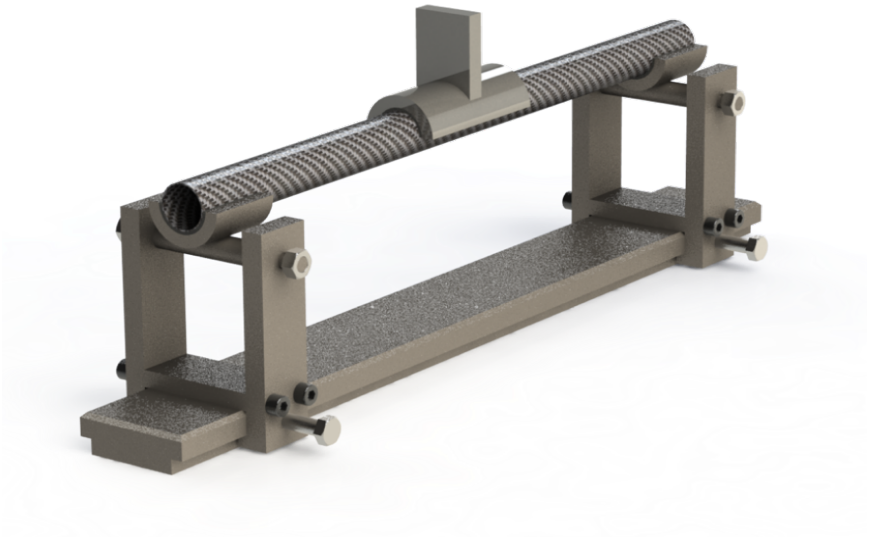

Figure 6: Designed rig

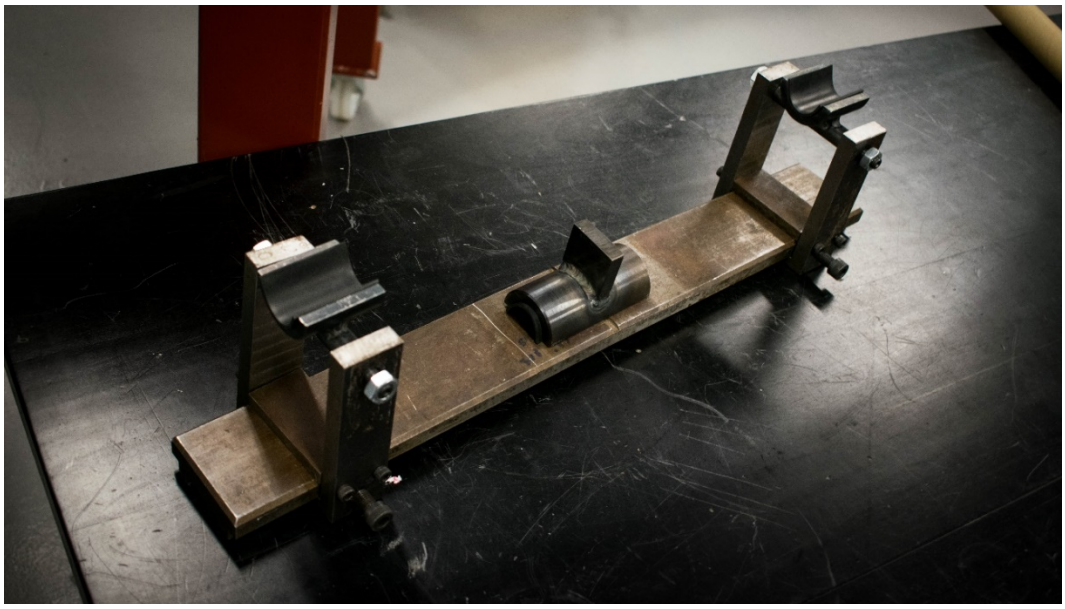

Figure 7: Manufactured rig

4.1.3. Measurement

The appropriate strain gauges were selected and carefully applied in those points where the strain data was required. Following the bending theory, the maximum bending moment and, consequently, stress and strain, will be obtained in the middle section of the tube. Then it decreases until zero at the ends, as it is seen in Figure 3. Test 1 was carried out as a first attempt to see how the tube, machine and fixtures were going to perform, only one gauge was applied, in the middle bottom of the tube (tensile side).

After this test, and knowing where the snap was produced, more gauges were applied in the section where the tube broke in the test 1, having strain data in both compressive and tensile sides. This allowed us to have a good understanding about the strain distribution in the tube. The data acquisition was carried out using the LabVIEW software. For all the tests, distance between gauges 2, 3 and 4 and the centre of the tube was 68 mm.

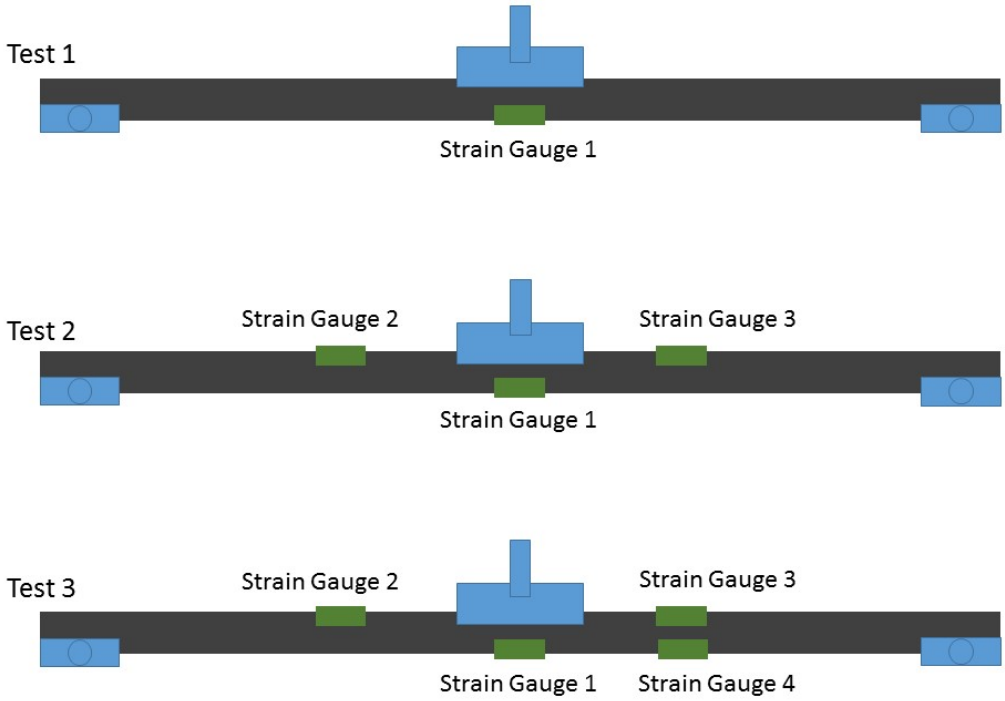

Figure 8: Strain gages positions on each test

With the objective of having visual information to analyse later, all the tests were video recorded, using both high speed and reflex camera. With the same purpose, all the broken tubes were photographed.

4.1.4. Results and conclusions

The outputs of the machine are the displacement of the nose and the force applied, both over time. The Figure 9 shows an almost linear evolution of the force over time. It has to be emphasised that at the beginning of the tests there is a non-linear behaviour due to the compression of the rubber on the supports. Another factor to take into account is the displacement that the rig experiences, being apparent in the first stage of test 2.

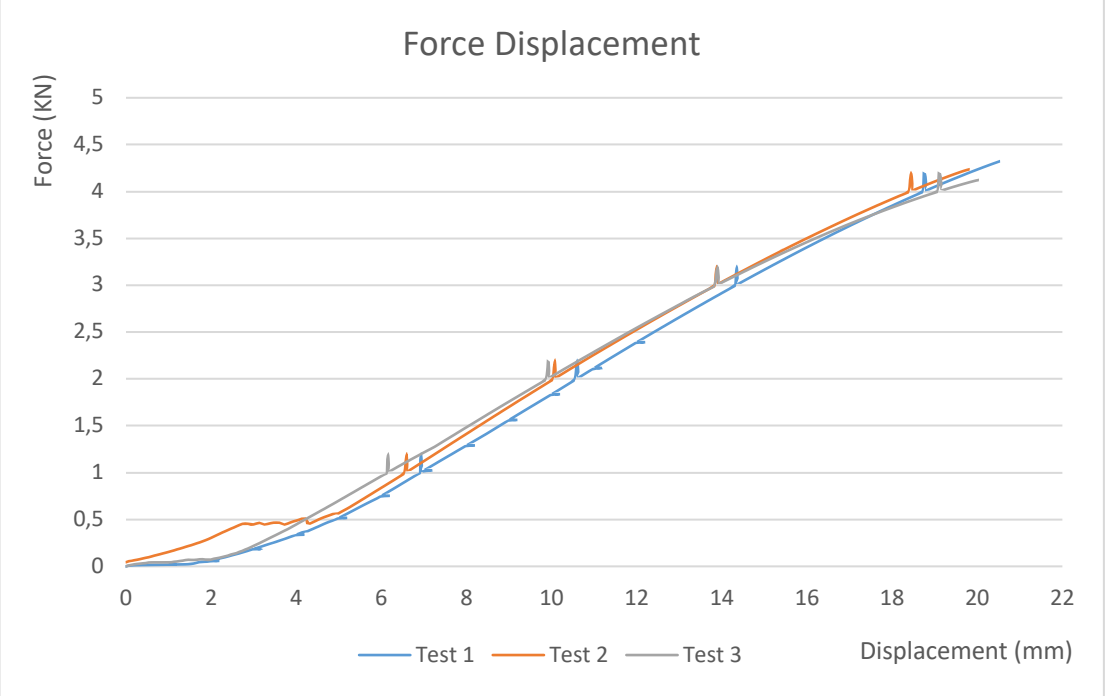

Figure 9: Force - displacement for each initial test

The Figure 9**,** also shows the expected behaviour of the carbon fibre tube. The force increases proportionality over time and then, suddenly, the tube snaps. No plastic behaviour is noticed.

Also, it can be noticed some little peaks along the curve. These peaks could be produced by the machine sensibility or by some other reasons.

In Table 4, the maximum force and the displacement of the nose at the moment just before the failure of the tube are shown for each test.

Table 4: Maximum force and displacement for each initial test

	Max. Force (KN)	Max. Displacement (mm)
Test 1	4.3	18.5
Test 2	4.2	17.8
Test 3	4.1	18

The strain gauges measured the strain over time. The Figure 10 is an illustration of the maximum strain values in each test. This data will be used when simulating the tube and layup with FE software.

The red line represents the section where the tube broke in each test. It can be appreciated that the three tubes broke more or less at the same distance of the edge of the nose (18 mm). The fracture was initially expected to occur in the middle of the tube as the bending moment in a 3-point bending test reaches its maximum in that point. Nonetheless, after the tube was tested, the failure point was located near the ends of the loading nose. With this in mind, it can be concluded that our test was effectively a 4-point bending test because, as the tube was bending, the contact with the surface of the nose gradually decreased until all the load was concentrated on its two edges.

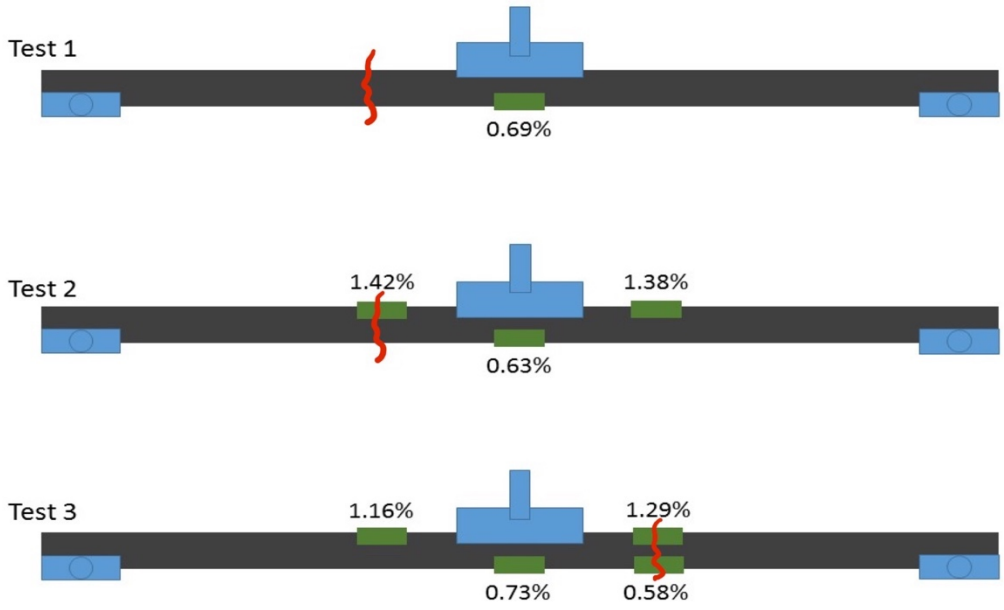

Figure 10: Maximum strain measured in the initial tests

From the examination of the broken tubes and the maximum strains, the failure mode can be deduced. All of the tubes failed in a similar way, with a sudden snap and

a big noise. After this catastrophic failure, the tube was divided in two parts, only slightly connected with each other on the tensile side. This confirms our prediction that the failure started on the compressive side, and then propagated through the entire section. Looking at the Figure 10, it can be understood why the tube did not break completely on the tensile side: the strain on this region was not high enough to complete the break. The Figure 11 shows this scenario.

These results and conclusions were used for the next part of the project, the simulation.

Figure 11: Initial test result in one tube

4.2. Simulation

For the simulation, ANSYS was used. While the initial tests on the naked bar were prepared, the member of the group responsible for the simulation started gaining knowledge of the composite extension of this software and preliminary work was done.

The main objective of these simulation analysis was to obtain the ultimate strain of each model. With this data, an appropriate material selection is conducted as well as their different configurations, to come up with some layup designs that behave as intended.

All the simulations had several points in common:

- First of them was the applied force, which should be similar to the original force where the tube was broken.
- Second one was the naked tube model preparation. In order to achieve the same failure behaviour, with similar strain and stress values, the properties of the default material had to be changed. The ultimate tensile stress was set up from 350 MPa to 4900 MPa, and Young Modulus from 61000 MPa to 39500 MPa.
- Third one was the boundary conditions, introduced in the initial tests section. On one side of the bar there is a pinned support (only Z rotation is allowed) and, in the other side, a roller support is placed (Z rotation and X displacement are allowed).

4.2.1. Original set up

Initially, the geometry of the naked tube, Figure 12, was designed on SolidWorks and then imported to ANSYS. This was done to prevent a possible interference between the supports and the tube.

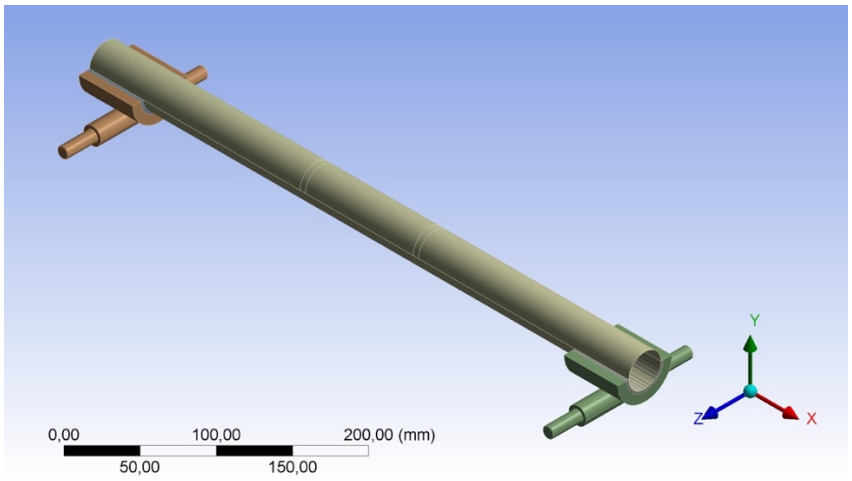

Figure 12: Geometry used for bending test

Then, the geometry was sent through ACP (pre) tool where the layups were added, as can be seen in Figure 13.

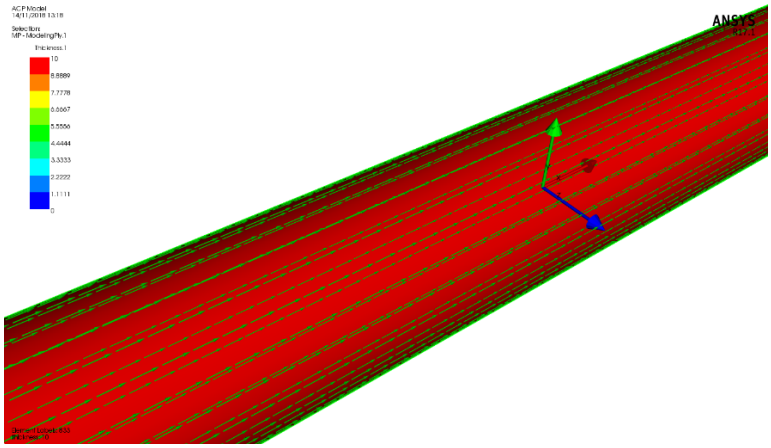

Figure 13: Fibres directions

The nose was not taken into account because it generated an error in the tensile region (possibly due to the loss of contact explained in 4.1.4), so it was necessary to be replaced by two pressures in the position where the nose made contact with the tube in the real experiment, Figure 14. Those regions of contact were simplified as two 5 mm wide strips that spanned across half of the cross-section perimeter.

Once this is done, the model of the naked tube was ready to be solved.

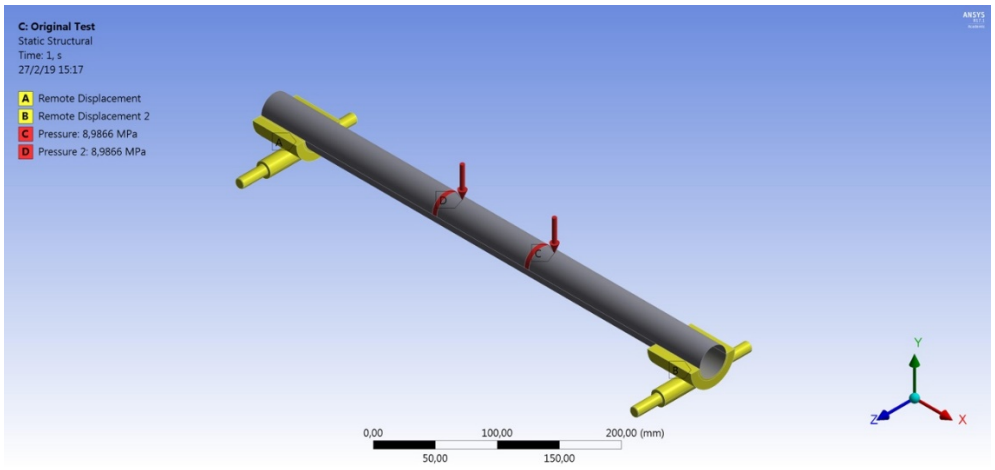

Figure 14: Test set-up

Results

In the following images, results are shown and discussed.

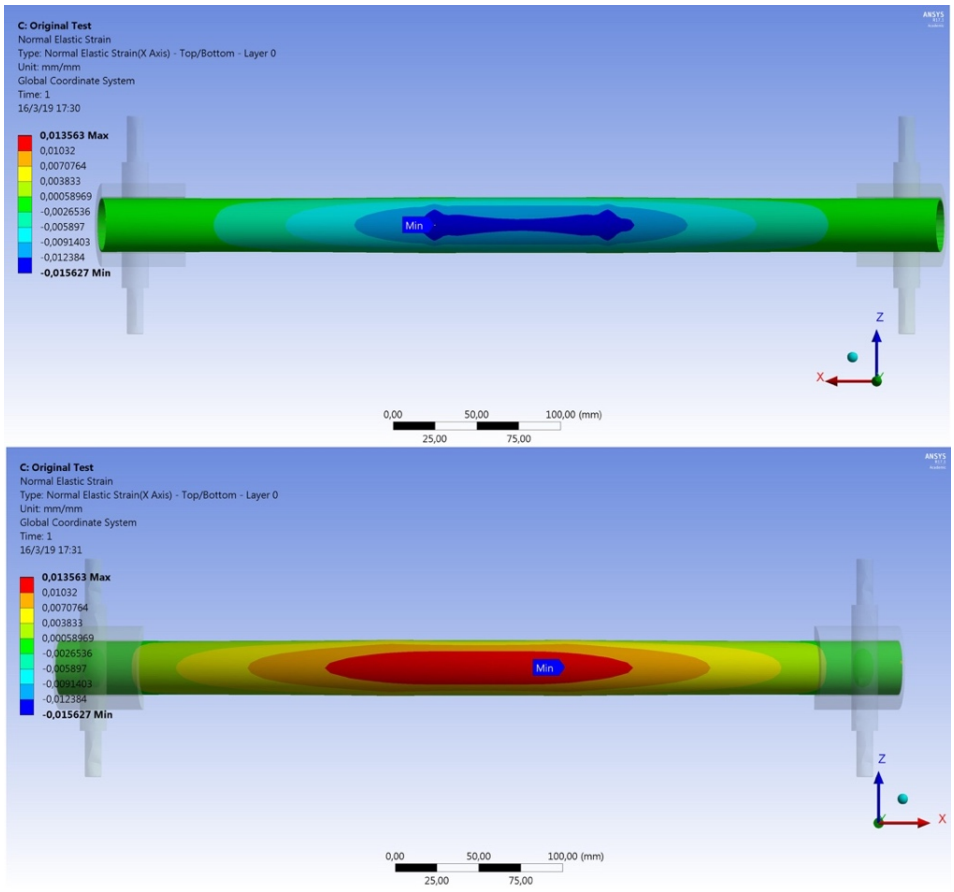

Figure 15: Strain in the naked tube

In Figure 15**,** strain on top and bottom of the tube can be seen, respectively. Thanks to the modifications applied to the material properties in the FEA simulation, the same ultimate strain was reached in both the simulation and the bending tests.

As it could be observed in the bending tests and later on confirmed by ANSYS, the strain in the compressive zone is larger than in the tensile one. Note that, in posterior simulation analysis, the negative values relate to compressive strain, whether positive ones refer to the tensile.

All the following layup designs were planned with the intent of achieving a failure initiated by tensile processes. The reasoning behind this decision is that this is the most predictable failure mechanism in composite materials, as is mostly dependent on the strength of the fibres, which is a known parameter depending of the type of composite used. Another important argument is that visual warnings of failure on the handlebar's layup had to be necessarily placed on top of it for the rider to notice. There, tensile mechanism occurs.

Shear failure was already addressed with the selected aspect ratio of support span vs. diameter of the tube. So, to promote the tensile failure, the compressive one had to be delayed.

In the next step a layup is created to come up with a solution.

4.2.2. Compressive layup

Two materials were tested for this layup, IM7 and T1000, both with similar results. This layup (represented on top) was 1mm thick in both cases.

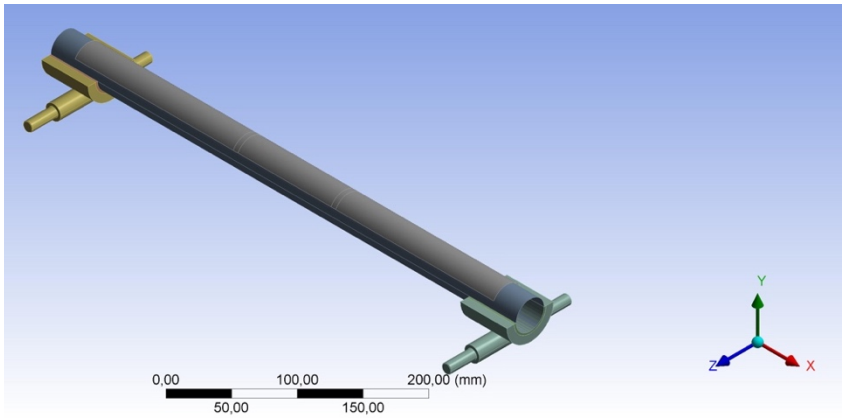

Figure 16: Compressive layer geometry

IM7

Using IM7, the following results were obtained.

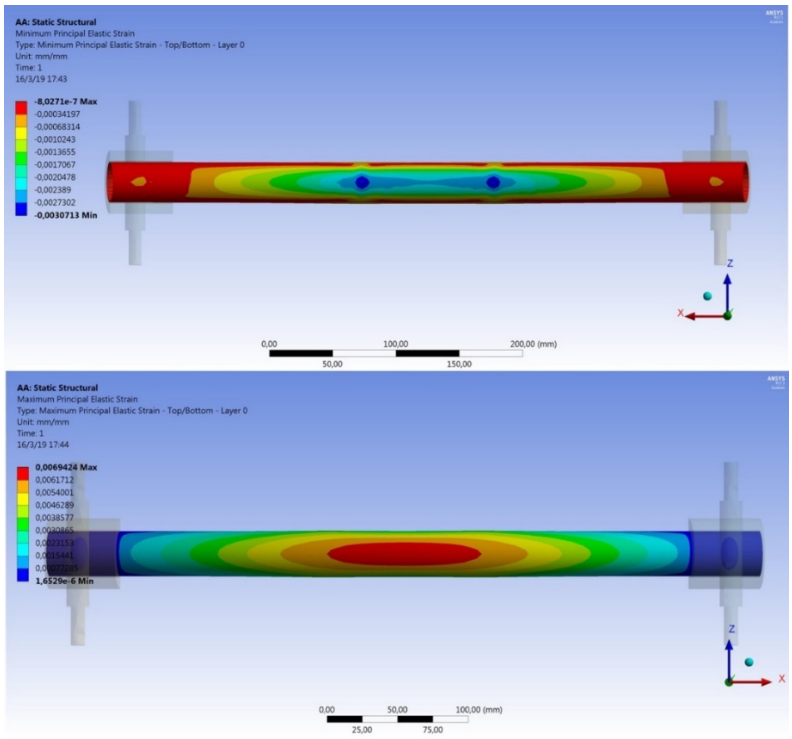

Figure 17: IM7 compressive layer. Strain in the tube

In Figure 17 strain distribution can be observed. The maximum strain on the tensile region is now greater than the minimum in the compressive zone, which relates to maximum compressive strain.

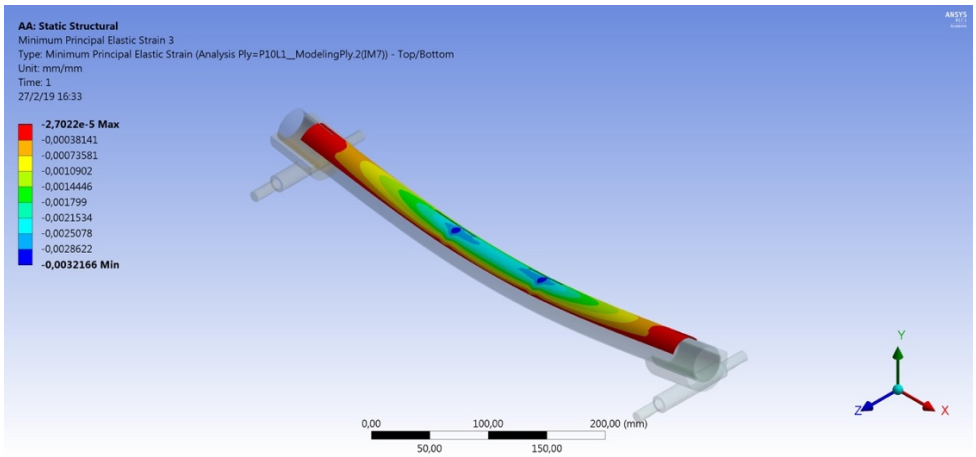

Figure 18: IM7 compressive layer. Strain in the compressive layer

In Figure 18 strain in the compressive layup can be seen.

T – 1000

With T1000, the following results were obtained.

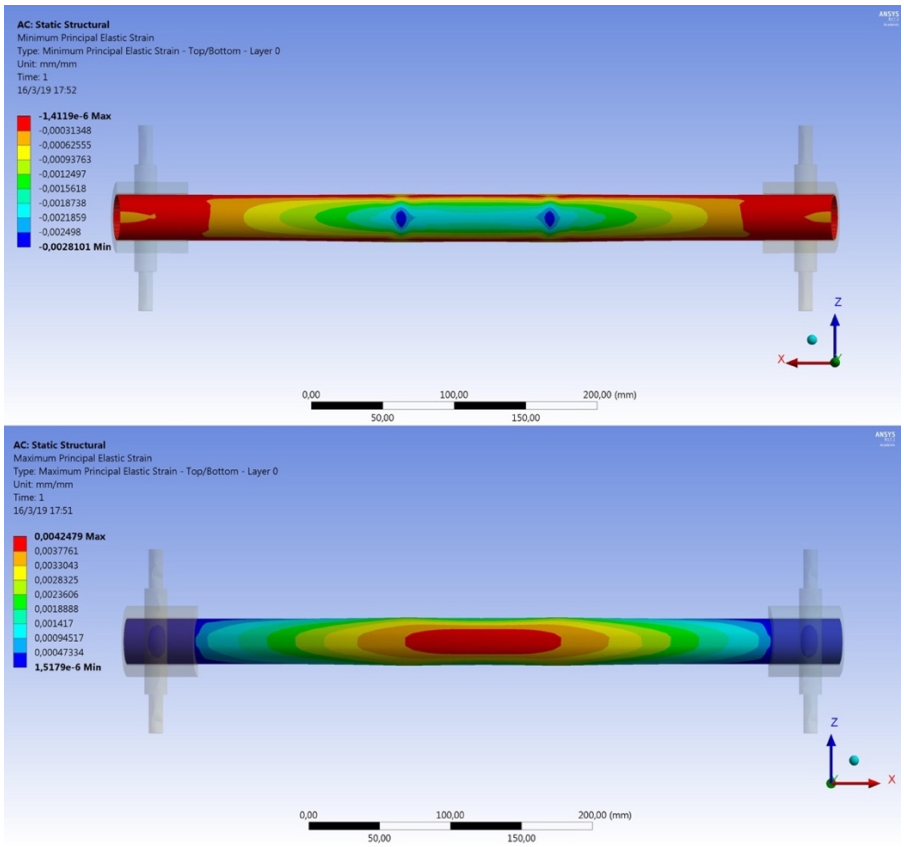

Figure 19: T1000 compressive layer. Strain in the tube

In Figure 20 the strain is shown. Maximum strain on the tensile part is now greater than the minimum in the compressive zone.

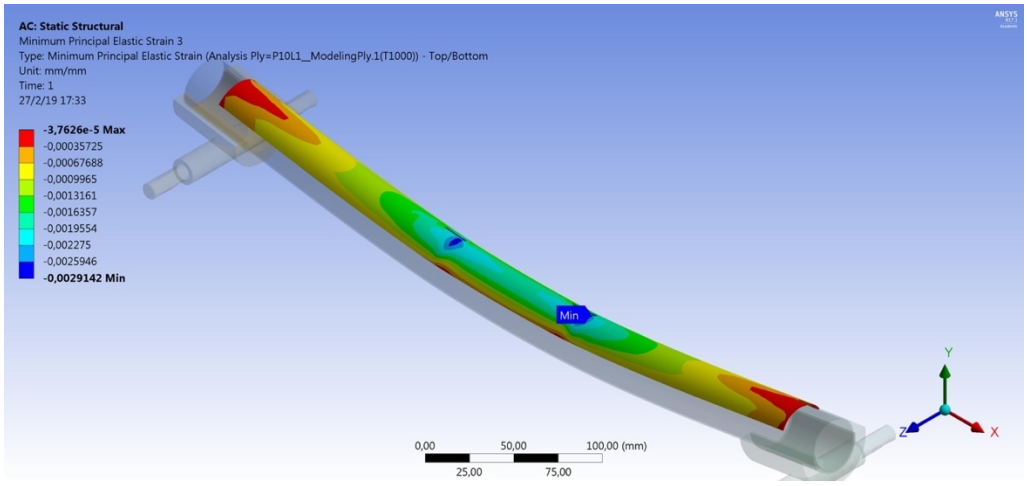

Figure 20: T1000 compressive layer. Strain in the compressive layer.

In the end, IM7 was chosen because it was available in the labs.

4.2.3. Final layups

Once the compressive failure issue was addressed, two different complete layups were created.

The geometry was built by adding another layup to the previous model, this time on the tensile side. There are only a few changes between the only compressive configuration and the complete one. In this geometry, both top and bottom layers had different thicknesses according to the layup that would be tested.

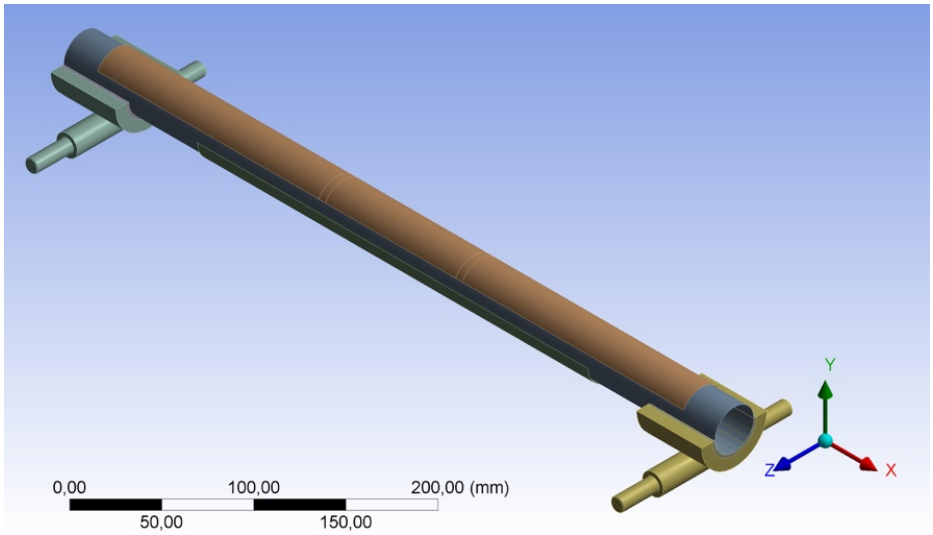

Figure 21: Complete layup geometry

Just before starting with the first layup, a brief explanation of the failure mode occurring in these layups is needed. The middle and the outer layers in the tensile side are set up to brake with enough energy that the entire layup peels off, as can be seen in the following image. The discontinued lines represent broken layers. In the first stage, YSH 70 is fragmented due its lower ultimate strain. Then, the reduction of fibres holding the stresses lead to the final failure of the IM7 layer. [3] [4] [5]

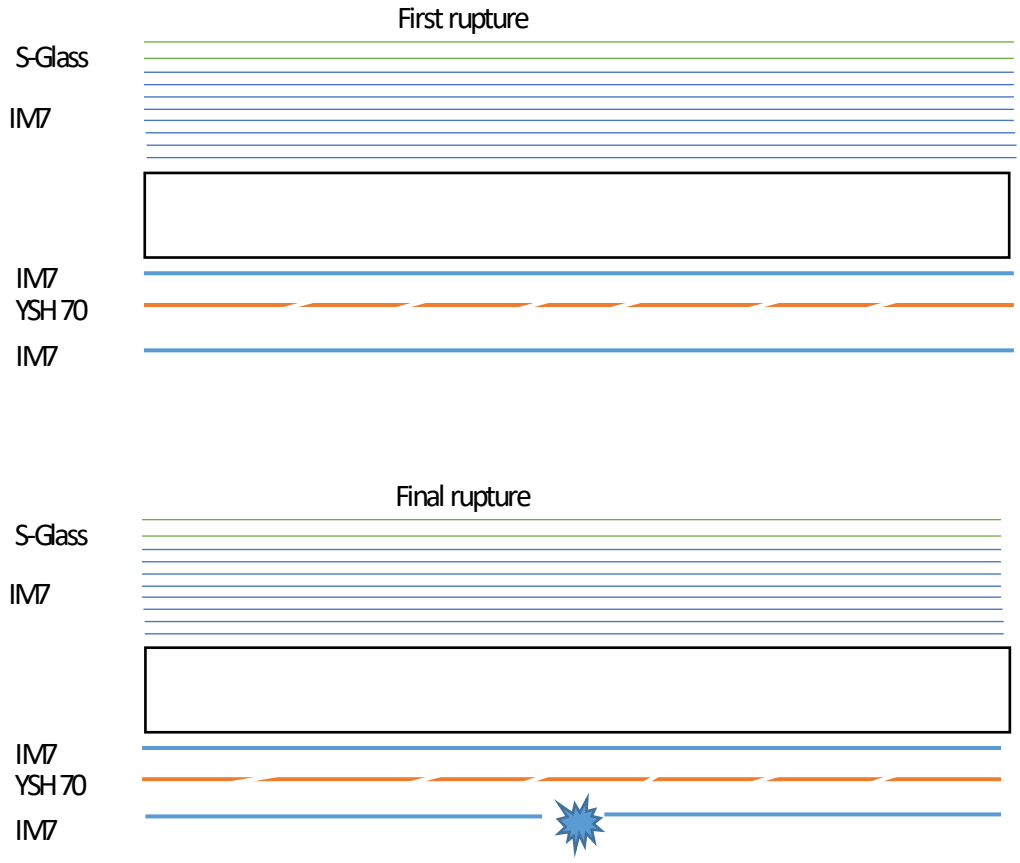

Figure 22: Rupture mode

In the moment the peel off effect happened, the bar would still carry load and the cyclist would have enough time to stop and get off the bicycle.

IM7 – YSH70 – IM7

This layup was composed by S-Glass and IM7 on the compressive side and IM7 and YSH 70 on the tensile region.

Figure 23: First layup design

In Figure 24, the strain in the top outer layer is shown. Here, S – Glass strain was 0.23% and the strain in IM7 was 0.21%, both in compression.

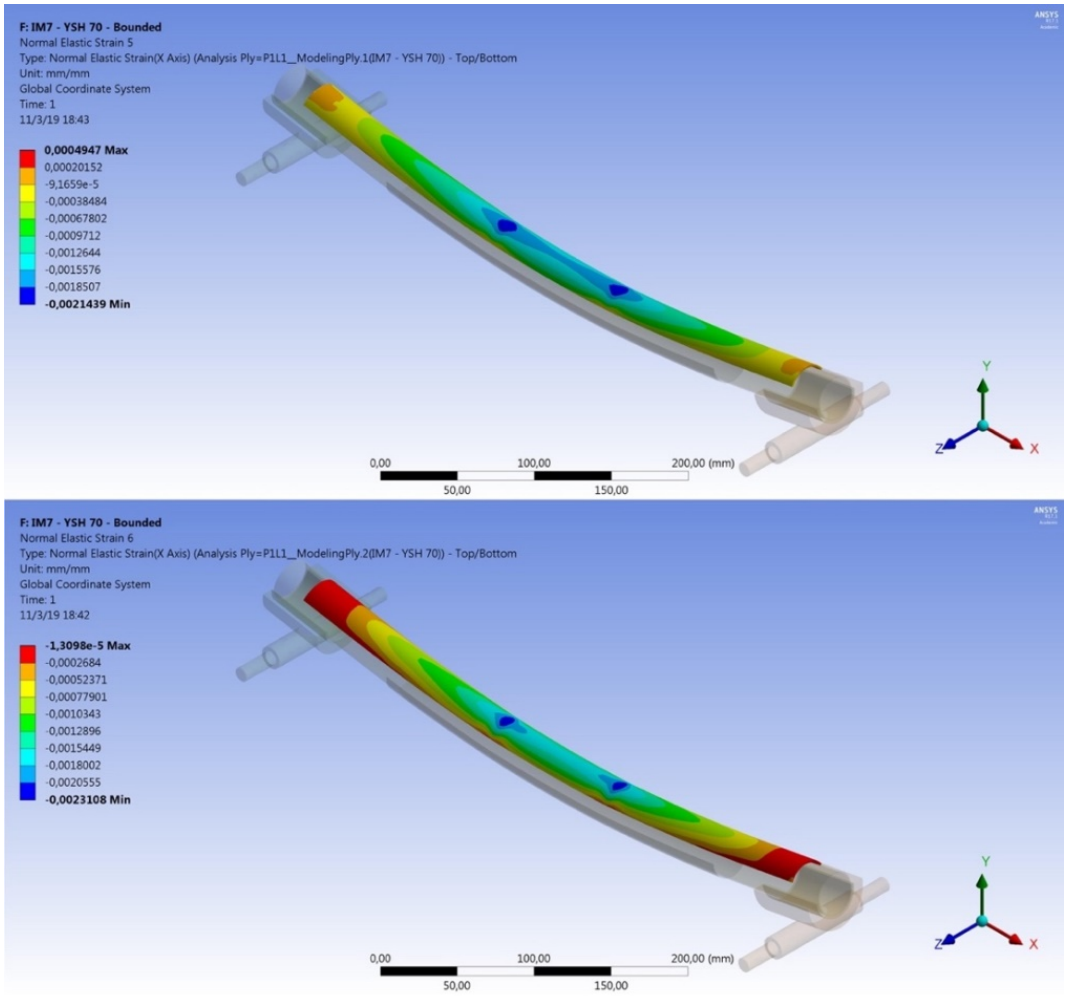

Figure 24: Top layer strain IM7 - YSH 70 - IM7

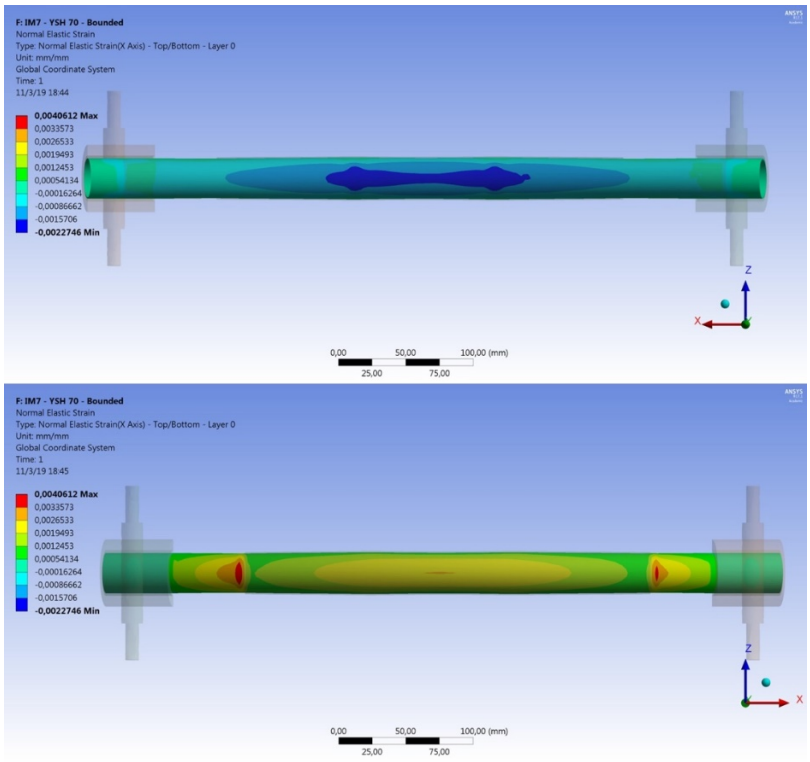

Figure 25: Tube strain IM7 - YSH 70 - IM7

In Figure 25, the strain of the tube is represented. The compressive strain was 0.227% and the tensile strain was 0.21%.

The length of the layers in the tensile part of the tube had to be reduced as, if they spanned across the whole tube, it caused interference with the supports.

As it can be seen in the tensile strain picture (Figure 25, bottom), high strain was apparent where the bottom layup ends. While manufacturing the layups and applying them onto the tube, this aspect should be considered. Each layer would need to be cut in decreasing lengths and applied to the tube as Figure 26 shows.

Figure 26: Gap between layers

In Figure 27, strains in the bottom layup for each one of the three layers are shown. The inner IM7 strain was 0.262%, the strain in the YSH 70 was 0.264% and the strain in the outer IM7 was 0.266%.

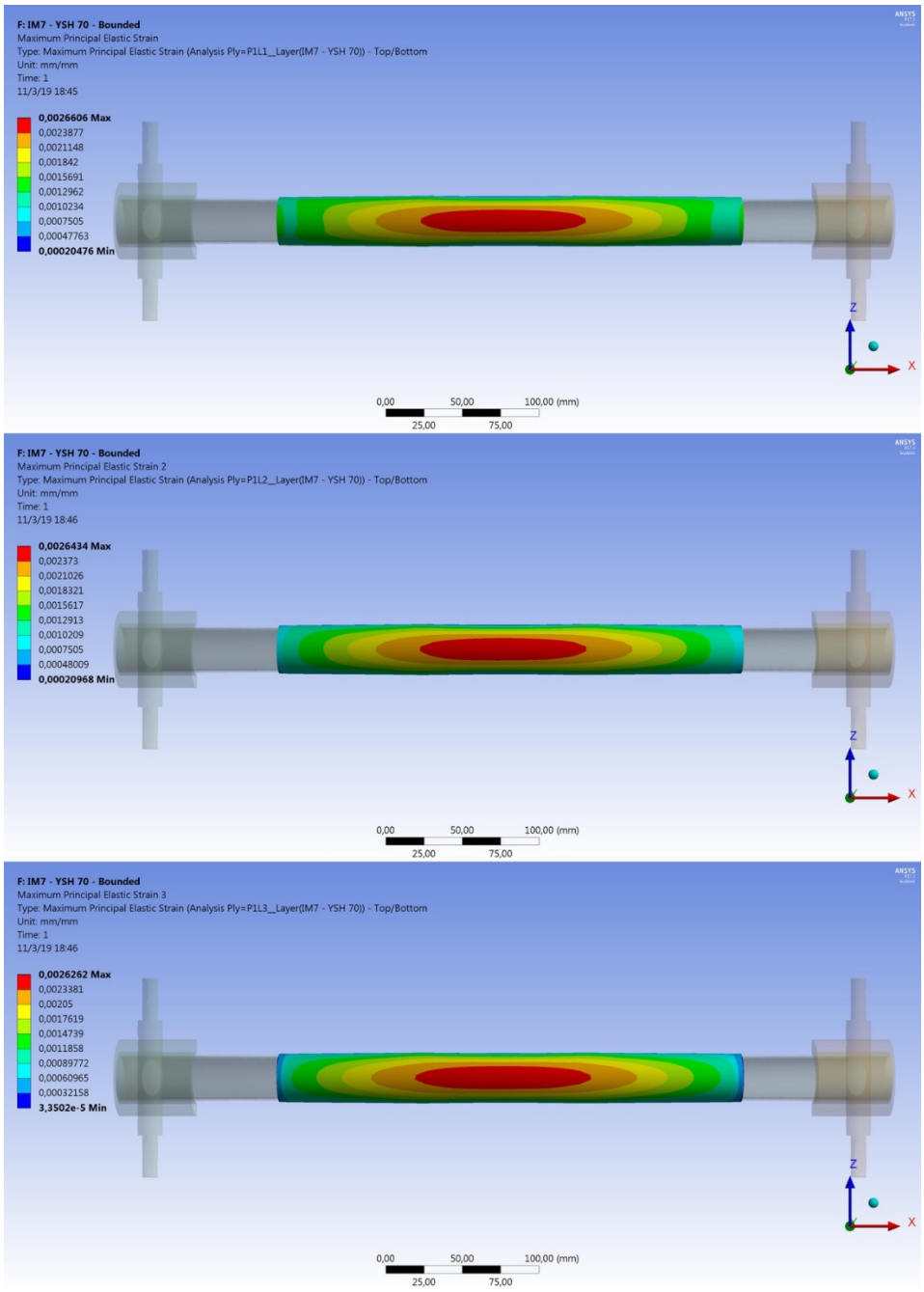

Figure 27: Bottom layer strain IM7 - YSH 70 - IM7

IM7 – YSH70 – YSH 70 - IM7

For the second layup, a second YSH 70 was added on the tensile zone and four IM7 in the compressive one. The final result was the layup that is sown below.

Figure 28: Second layup design

In Figure 29, the strain in the top layer can be seen. The S – Glass strain was 0.17% and the strain in the IM7 layer was 0.13%.

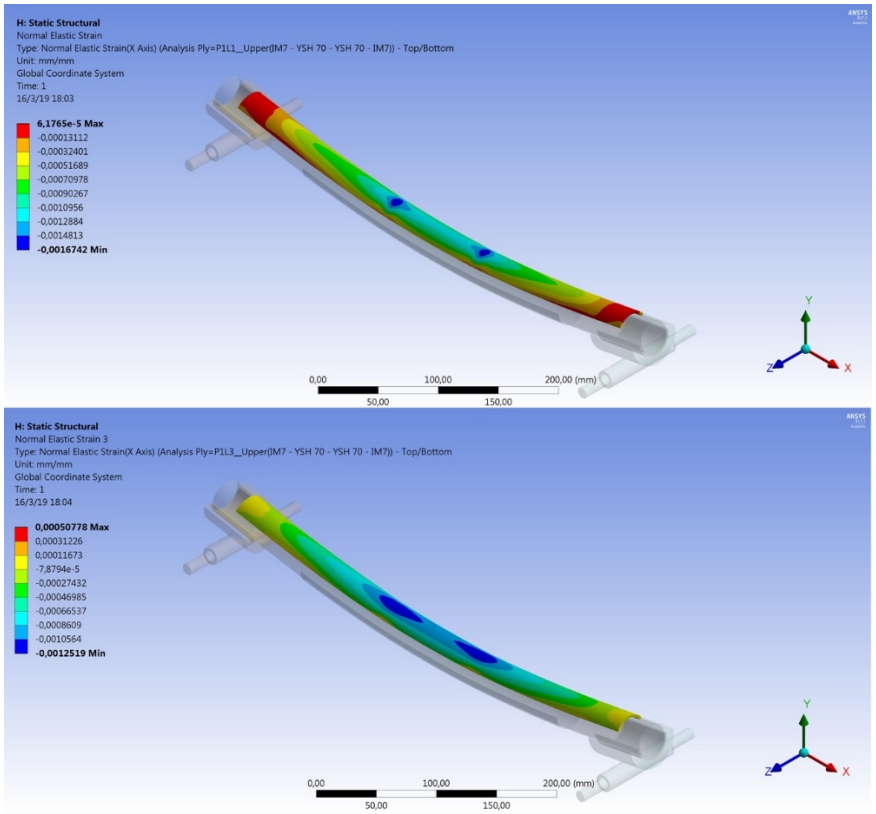

Figure 29: Top layer strain IM7 – YSH70 - YSH 70 - IM7

In Figure 30, the strain in the tube. The compressive strain was 0.165% and the strain in tension was 0.01%. As in the top layer strain, compression strain was represented by the negative sign.

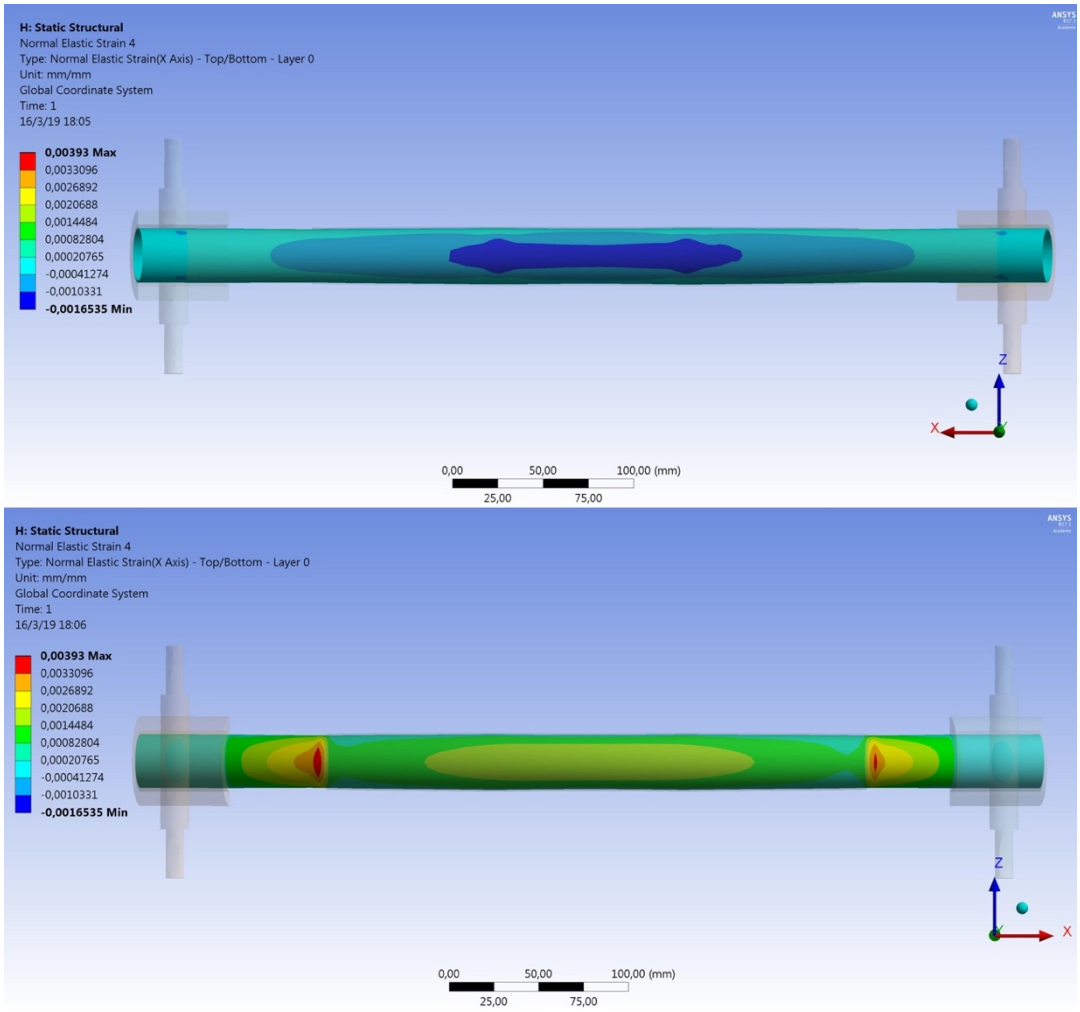

Figure 30: Tube strain IM7 – YSH70 - YSH 70 - IM7

In Figure 30, strains in the bottom layup for each one of the four layers are shown. The first IM7 strain was 0.193%, the strain in the first YSH 70 was 0.192%, 0.191% in the second YSH 70 and the strain in the last IM7 was 0.189% all in tension.

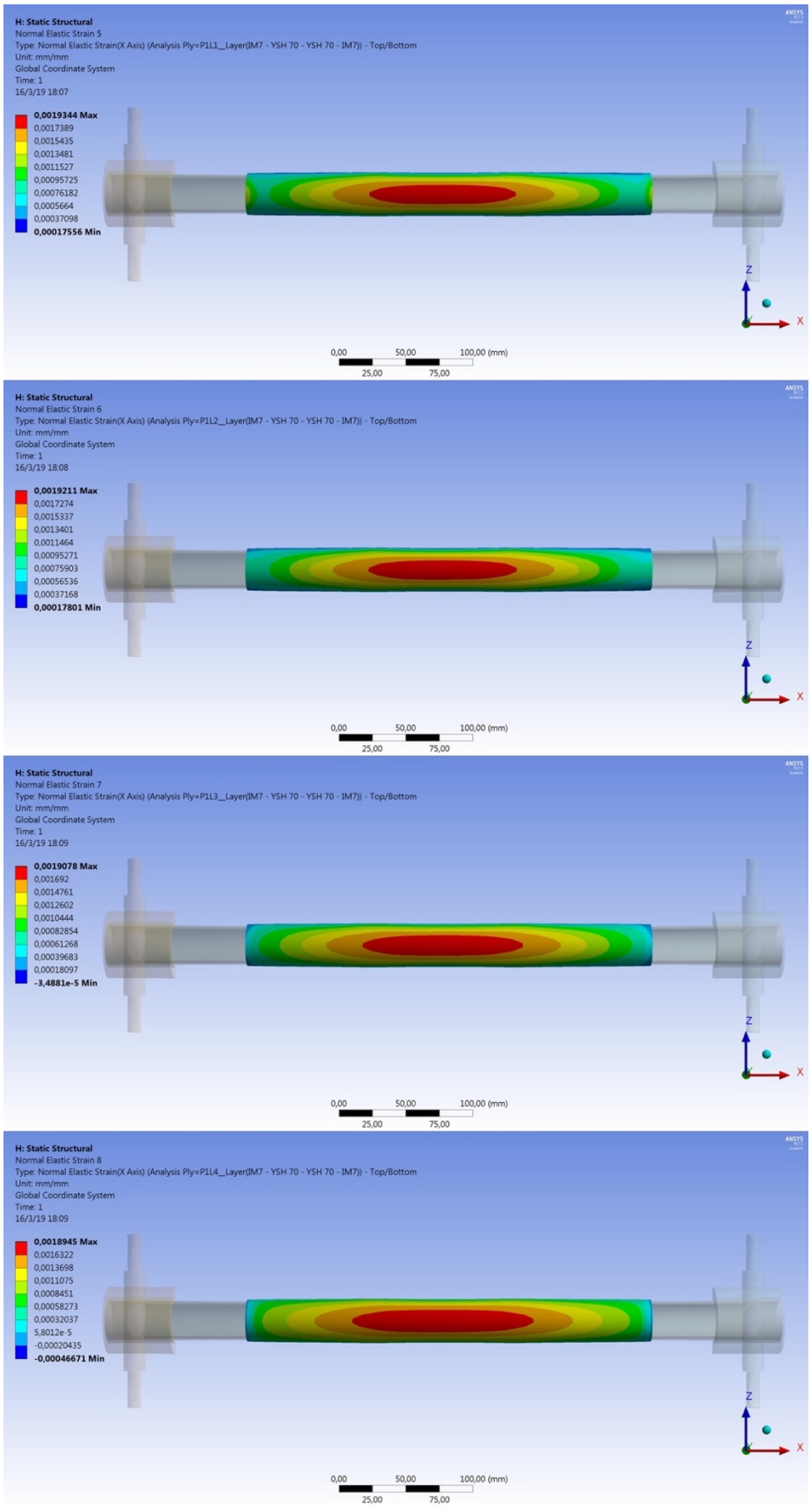

Figure 31: Bottom layer strain IM7 - YSH 70 - YSH 70 - IM7

We have chosen these two options for the following reasons:

- Two different approaches: a conservative option, which is the first layup where the difference in tensile strain between the bottom layers was bigger; and a riskier one, the second, where the difference in tensile strain between the bottom layers was lower.
- Both layups needed less material, so it was cheaper and quicker to manufacture.

From now on, the first layup (IM7 – YSH70 – IM7) and the second (IM7 – YSH70 – YSH 70 - IM7) will be referred in this report as layup 1 and layup 2, respectively.

4.3. Manufacturing

Once the two layups had been chosen from ANSYS, the manufacturing of these could begin. The two layups to be manufactured are:

Layup 1

- Compressive/top side of bar	→	3 S-Glass Layers
	→	10 IM7 Layers
-Tensile/bottom side of bar	→	2 IM7 Layers
	→	1 YSH70 Layer

Layup 2

- Compressive/top side of bar	→	3 S-Glass Layers
	→	14 IM7 Layers
-Tensile/bottom side of bar	→	2 IM7 Layers
	→	2 YSH70 Layers

The justification not to have the entire tube covered with the layup can be split into three main reasons.

- IM7 stripes that were available at the manufacturing lab only were 400 mm long, which is shorter than the tube.
- It saved time manufacturing because as shorter the layer, easier to place in the right position.
- ANSYS did not show great amounts of stresses and strains in these areas.

The method of manufacturing used to bond these layups together and to the CF bar was through Vacuum bagging. This method works by layering the Prepreg layup sheets over the mould or in this case the CF tube. Prepreg material is a composite material where the fibres have the polymer matrix pre-impregnated into the material. The vacuum bag then covers the layered composite and seals around the component with a vacuum pulling onto the material. This compresses the layers onto the tube. It is then heated within an autoclave under a specific heat cycle relative to

the pre-impregnated matrix conditions. The autoclave will be pressurised to further increase the pressure on the layered material to improve the bonding during curing.

With the layer material chosen the dimensions were drawn up and cut out of the prepreg sheets using a sharp Stanley knife with a safety ruler, it is important adequate pressure is applied during cutting to ensure a clean cut of the carbon fibres.

Layers were cut in order from tube surface out, meaning the layers were reducing in 10mm in length for each cut to ensure the desired 5mm step decrease in length between either side of the layers to induce a load spread throughout the layup when being tested. For example, Layup 1, the layer on the top of the tube was cut at 380mm length × 45mm wide; through 13 compressive layers the top layup layer of S-Glass came to 260mm length × 45 mm wide to ensure the required layer step decrease to the outer surface. This is illustrated in the figure 27b where the reduced layer lengths can be seen from the finished product.

Furthermore, during dimension drawing and cutting, it is considered that the material should be unsealed and out of the freezer for relatively short times as this can cause the prepreg sheets to dry out and age faster as they are uncured.

With the layers cut the CF bar must be prepared for application of the layers. This surface of the bar is sanded to create a relatively rough surface. Care must be taken to ensure the bar is not over sanded which would result in the outer matrix layer being sanded off and sanding the actual carbon fibres away. This can be gauged on the colour of the residue on the sand paper. White being degradation of the matrix, however black residue would mean the CF layers have been reached.

With the surface roughened- to increase quality of adhesion of prepreg layers to the CF bar- the surface must be cleaned. Acetone was impinged over the entire outer surface of the bar and then wiped over to remove the sanding residue and any other oils from human hand contact which could reduce the bonding strength. This was carried out often 2 to 3 times until the cloth was clean after wiping to ensure all residue is removed. From this point on it is vital to wear rubber gloves when handling the bar to avoid any oil on the surface from human contact before curing.

After cleaning the layers can be added to the CF tube. This ideally requires two people; one person to line up the bar and to use a steel rule to show wear the centre and end of the applied layer should be applied to the tube as well as to show placement for the stepped layup. The other person will apply the layer. This is a difficult task and a method was required created due to only having a practical tutorial on flat surface applications. For application to a tube, the applier will place the middle of the end of a layer onto the correct part on the tube, they will then run their finger along the top of the tube pressing the middle line of the layer onto the

tube, whilst keeping elevated tension on the unapplied part to ensure a tight fit without creases or air bubbles. Once the middle of the entire length of the prepreg has been pressed by the finger; the finger will run across the centre of the added layer down the sides of the layup to attach the entire surface of the layup. After this some time should be taken to press every part of the prepreg into the surface pushing with relative force along the length to remove any trapped air between the surfaces. This is then repeated for all the layers.

With this a method for vacuum bagging the tube had to be made. One considered way is to completely cover the entire tube in the vacuum bag and would make sizing the bag much easier. However, this would induce a lot of pressure on the original CF tube, with vacuum pressure and autoclave outer pressure pressing around the tube.

The other method which is created for the implementation of the project was to seal the vacuum bag around the perimeter of the layup and not the entire tube. This means the pressure exerted on tube during curing is less with the vacuum pressure only being exerted as the autoclave pressure can run throughout the tube.

The first step of vacuum bagging is to cut the release film material to cover the surface area of the layup. This prevents the materials within the vacuum bag sticking to the layer and ruining the surface of the prepreg as well as making the release of the bag from the tube easier. With this, cotton cloth was cut and wrapped around the prepreg area with the release film around it.More cloth is placed running off the circular tube and flat out to the side of the tube. The vacuum bag is then cut and fitted with sealant tape, as can be observed in Figure 32

Figure 32: Detailed view of the sealing tape around the tube

This is then wrapped around the cotton covering the layup and then out to the side where the cotton extends. This then gives space to fit the vacuum plug to the bag, as is shown in Figure 33. Once this is fitted the sealant tape is pressed around the perimeter to create an isolated, sealed environment around the applied layers as shown below.

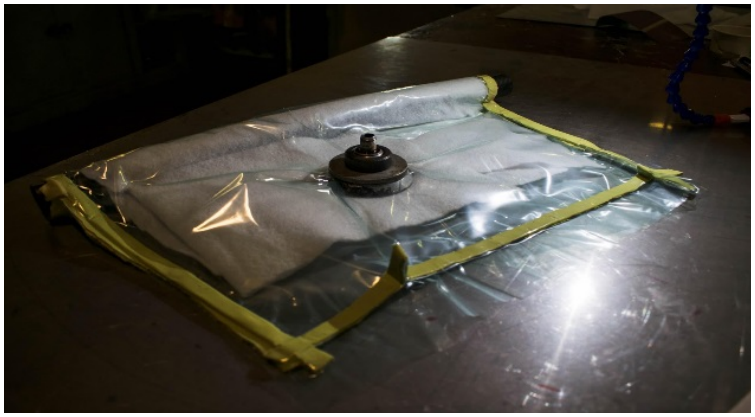

Figure 33: Vacuum bag sealed

This is the result of the vacuum bag technique implemented by the team to ensure successful curing and adhesion on the tube surface. The cotton plays two roles in the process. One is it allows efficient spreading of the vacuum and provides a medium for the vacuum to run from the plug to the Layers around the tube. The second role is that is absorbs any excess resin released from the prepregs to avoid uneven resin distribution during curing.

With this, the bag is tested for sufficient vacuum performance. The plug is linked to the autoclave vacuum pumps, at first it is common to hear a hissing which means there are gaps in the sealant. The sealant is pressed and worked until the hissing stops and is continued whilst checking the vacuum gauge to watch for improvements. Once the vacuum is sufficient at around 0.6 bar the seal is good enough for the autoclave.

The cure cycle for these layups was implemented due to the cure cycle for the epoxy resin within the IM7 prepregs. The epoxy is the Hexcel 8552 product and means the heat cycle for the implementation of our layup is as follows.

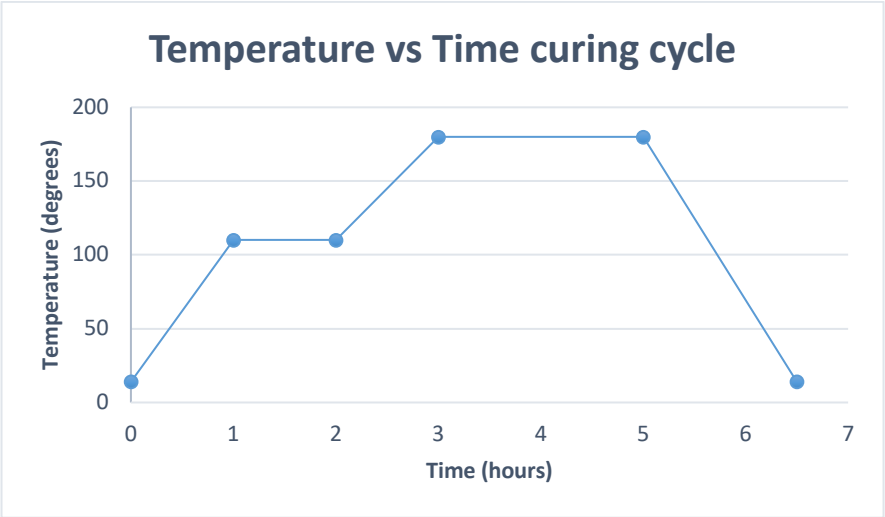

Figure 34: Cure cycle graph

When the autoclave is closed the vacuum is remained on the material. The pressure begins to increase in the autoclave to 3 bar when the heaters are turned on. The cure cycle rises at just below 2 ˚C per minute to 110˚C within the first hour and sits at this 110 ˚C for an hour, it then rises at closer to 1 ˚C rise per minute to 180 ˚C where it will sit at for 2 hours. After this the temperature slowly reduces to room temperature between 2-5 ˚C per minute to prevent cracking due to thermal shock. Once it has been cooled, and the sealant has cooled the vacuum bagging with the cotton and release film may be removed resulting in the end product. The cure graph can be seen in Figure 34.

Figure 35: Tube finished

Figure 35 shows the different stepped layers reducing in length towards the outer surface of the layup. The dark material is the IM7 and the orange coloured layers are

the Glass fibre prepreg layers. Looking onto ways to improve the method would be to carry out further work into improving the finish of the end product. This may be achieved by introducing another layer within the vacuum bag to reduce the patterned finish on the prepreg. This is due to the cotton fabric being pressed against the prepregs during curing imprinting the cotton roughness on it. However, since the main aim was on the performance of the layup in the bending test, perfection in the surface finish was not a main aim.

Table 5: Tube properties before and after the manufacturing

	Naked bar	Layup 1	Layup 2
Weight	68 grams	116 grams	132 grams
Increase in weight	-	70%	90%

4.4. Final tests

The two manufactured layups were tested in a bending test, at least at the beginning with the same setup as the initial tests done on the naked tube. Same displacement velocity and same span. The objective of this test was to confirm that the predicted gradual failure had been achieved, in opposition with the sudden snap obtained in the initial tests. Video recording was carried out.

A total of three reinforced tubes were tested. Test 1 and test 2 were done on tubes with the Layup 1, and test 3 on the tube with the Layup 2.

4.4.1. Layup 1

Test 1

The setup of this test is shown in Figure 36.

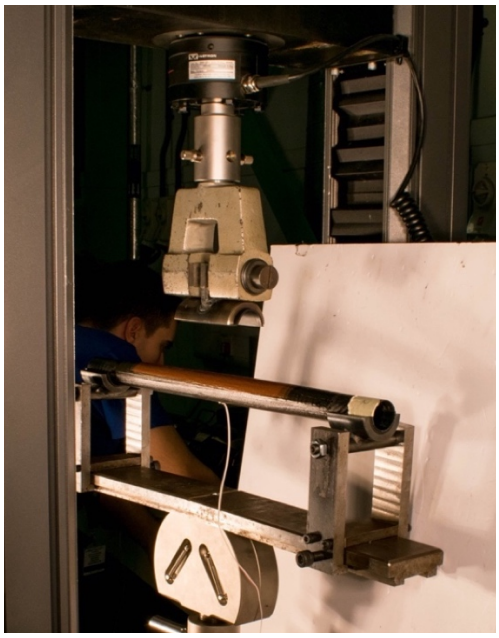

Figure 36: Test 1 set up

At first sight, during the test, the tube was showing a very stiff behaviour. The force was increasing as shows the Figure 37, exceeding the 4300 N of maximum force obtained in the initial tests. When it reached 7500 N, the tube crashed exactly in one of the edges of the layup. The most reasonable explanation of this failure is that, since the edge of the layup was not over the supports' surface and being consequently

under high shear stresses, the stress concentration generated in this area promoted the failure of the tube.

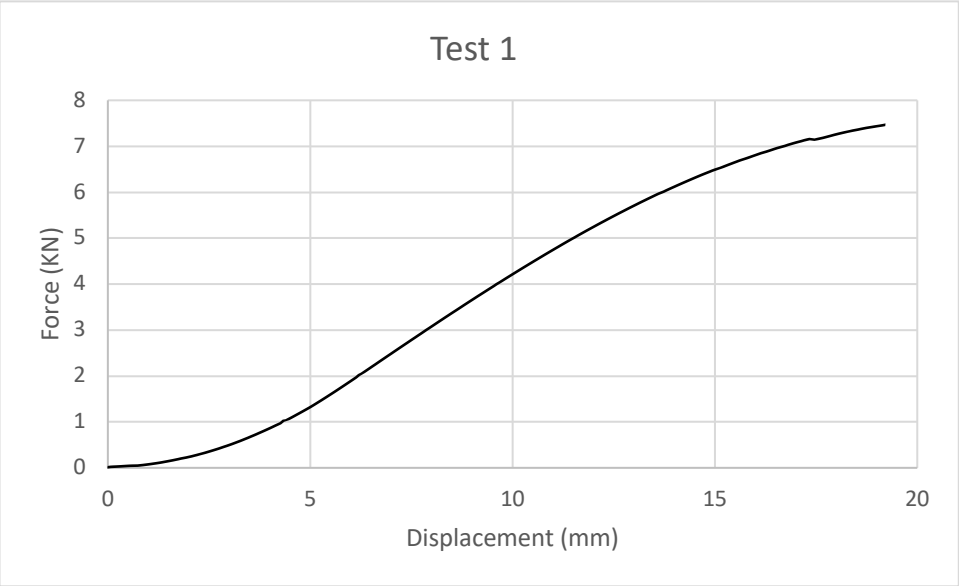

Figure 37. Force – displacement Test 1

It is important to say that, in contrast with the result of the initial tests, the tube achieved a certain pseudo-ductile behaviour before the final and sudden snap. One evidence is that the curve shows now less linear progression. Also, the breaking noises from the internal fibres of the layup, and the fact that the tube was not completely separated in two pieces after the final failure, were sign and evidence, respectively, of this behaviour. Figure 38.

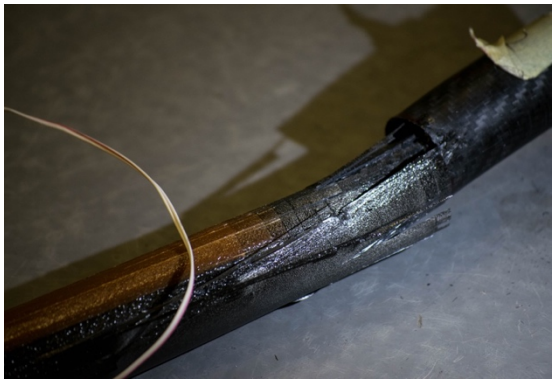

Figure 38: Test 1 tube snap

Although some gradual failure was apparent, the objective was not entirely reached. After examining the broken tube, the external part of the layup did not show any sign of fracture.

Test 2

Taking into account the result of the previous test, one challenge now appeared. On the one hand, the span had to be reduced to avoid having tube with no layup under load, obtaining again the same failure. On the other hand, if the new span was reduced too much, the aspect ratio would decrease, having now a higher probability of achieving shear prematurely, even on the part of the tube with layup.

Finally, after thinking thoroughly about this, the testing team took the decision of reducing the span from 450 mm to 350 mm, having now this region over the supports´ surface. The decrease of the aspect ratio was taken into account, being in any case higher than 10. This new setup is shown in Figure 39 and Figure 40.

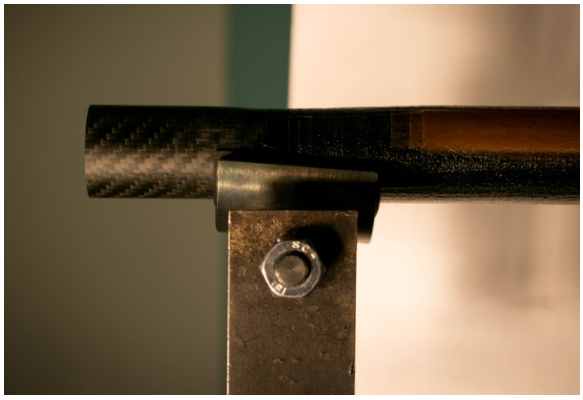

Figure 39: Test 2 set up, detail on the support

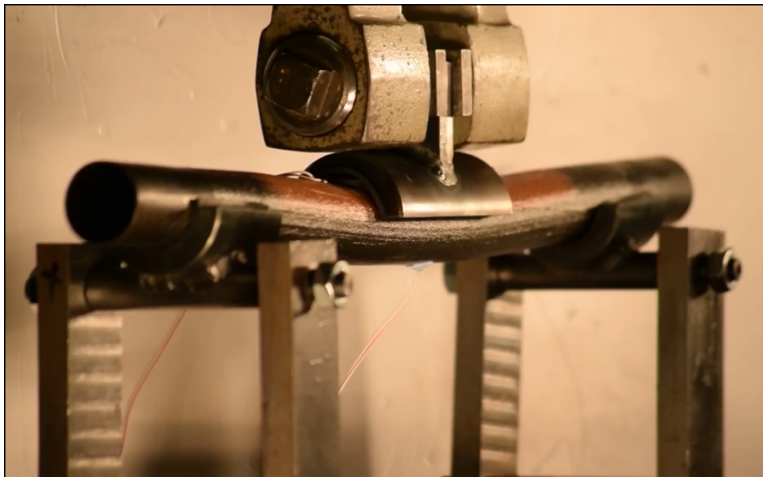

Figure 40: Test 2 set up

Comparing the Force – Displacement curve on the Figure 41 with the one of the previous tests, it is noticeable that more ductile behaviour was obtained in this reinforced tube compared to the previous one. In any case, it was not the wanted result. No visual warnings were observed.

However, noises during the test could be heard from 3000 N of load to the end of the test as a result of this certain gradual failure. Regarding to the maximum load, after the tube reached almost 10000 N of force, it crashed in one side due to, apparently, shear stress.

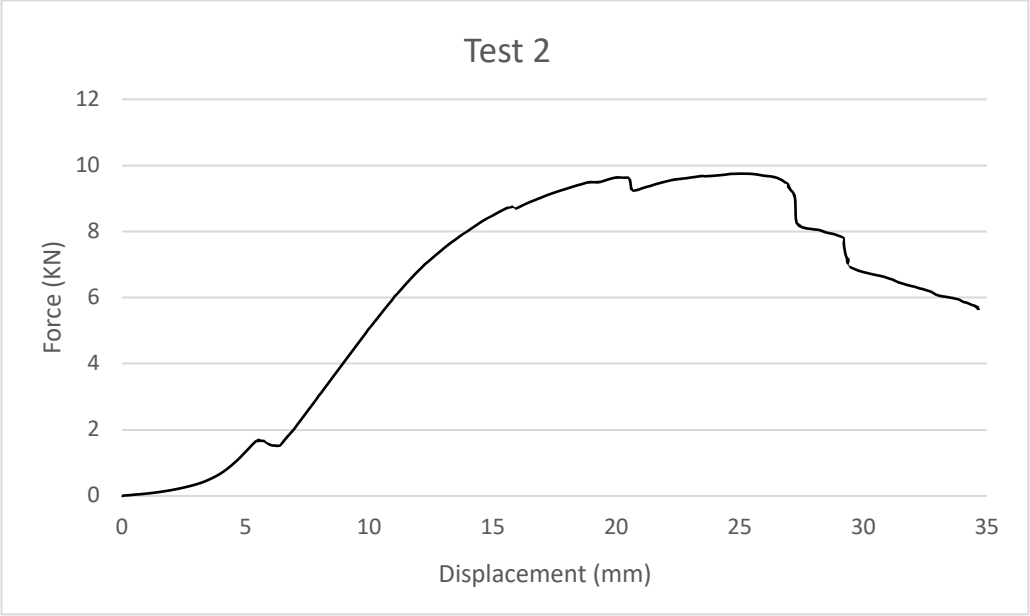

Figure 41. Force – time Test 2

After the break, the tube remained in one piece. Figure 42.

Figure 42: Test 2 result on the tube

4.4.2. Layup 2

Test 3

The second layup designed was tested in the same conditions as in the previous test, maintaining the span of 350 mm. In the same way as in the two previous tests, some noises were heard from 3000 N of force until the end. As it can be seen in the Figure 43, the tube withstood 11000 N before the final break. While the nose was descending, the force was linearly increasing until reaching around 8000 N. After that point, it described a curve, showing the wanted gradual failure before the snap.

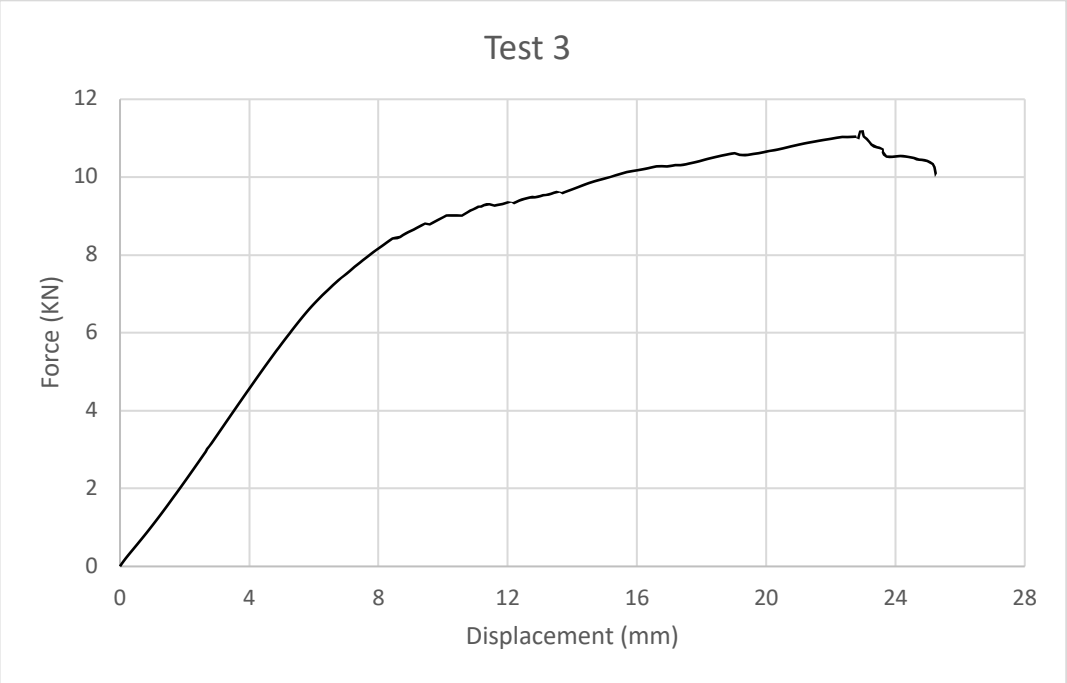

Figure 43. Force – Displacement Test 3

During the test, visual warnings that the gradual failure was happening were noticeable. Some parts of the external layer peeled off from the tensile zone as the load was increasing. Figure 44 shows this.

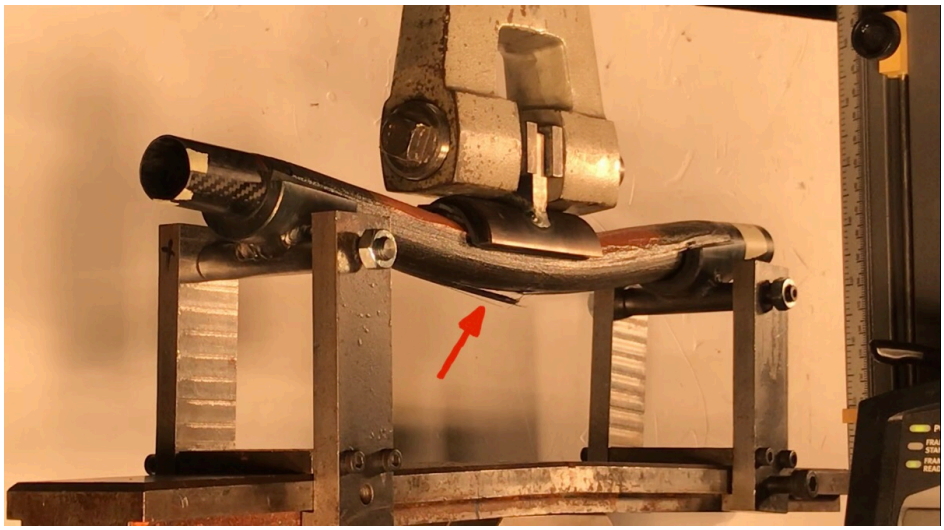

Figure 44: Test 3 gradual failure

It also has to be mentioned the high stiffness of this layup, noticeable in both Figure 43 and Figure 44. It is so stiff that does not allow the tube to bend.

In order to sum up the results of the three tests, the Table 6 is created.

Table 6: Final tests results

Test 1	No gradual failure	-	-
Test 2	Gradual failure	No visual warning	Audible warning
Test 3	Gradual failure	Visual warning	Audible warning

Looking at these results it can be said that the Layup 2 shows the best result.

5. Discussion

Initial and final tests results will be discussed and compared. On the one hand, in the first set of tests, carried up on tubes without layup, these broke in a catastrophic manner and no warnings were perceived. On the other hand, the set of tubes with layup showed a different behaviour where broken in the final tests.

As in the initial tests all the Force – Displacement graphs are similar, the curve of the test 2 is chosen to represent them. At the same time, the three of the final tests showed certain level of gradual failure, being the last, the most representative one. These both graphs are shown in Figure 45.

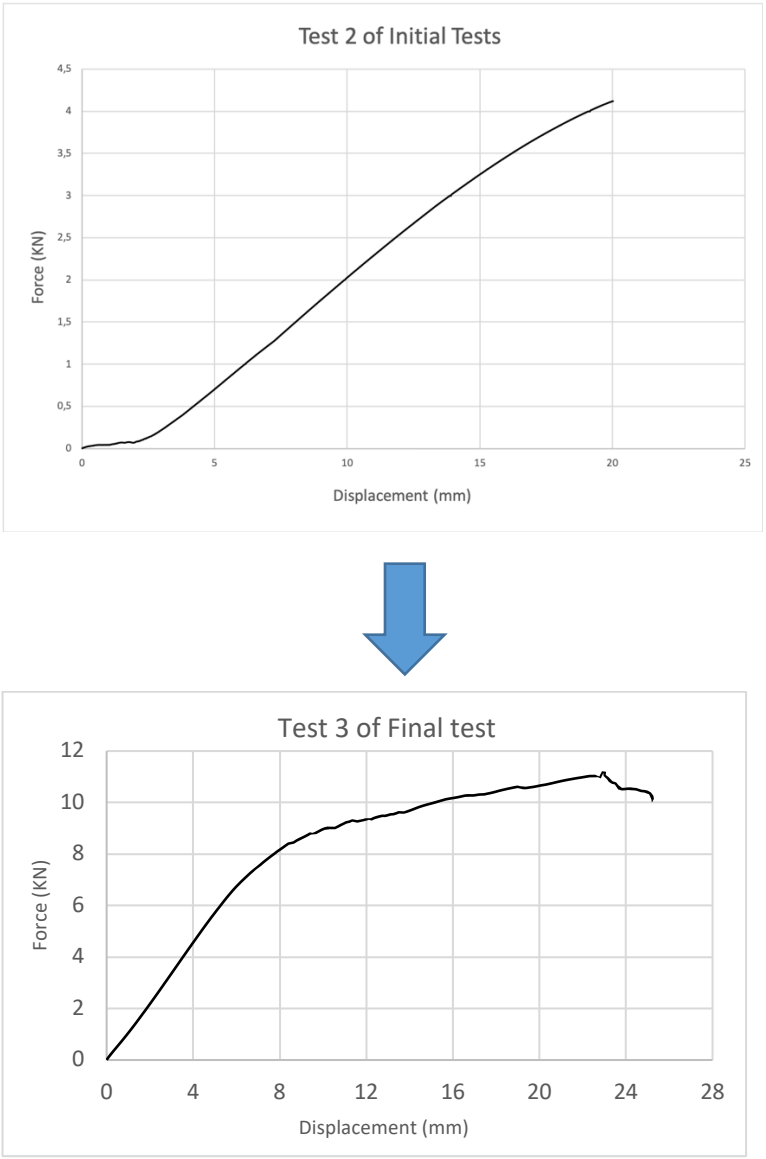

Figure 45: Comparison between initial and final tests

It can be seen in the initial set of tests the expected force displacement graphs for CF composites, a straight-line, occurring then the sudden failure. However, the second set of tests achieved a pseudo-ductile behaviour. Between force values of 0 and 7 KN the bar experiences elastic deformation. Beyond this point, the bar layup begins to fail before the tube. This curvature in the graph beyond 7 KN represents fibres within the YSH70 layers failing which results in loud cracking noises from the tube. This continues with fibre pull out and failure throughout the prepreg layers. This provides both visual warning with broken fibres fanning from the tube; sound of the fibres snapping and pulling out; as well as promoting greater deflection mirroring the behaviour of a yielding steel handlebar. This effect is shown in Figure 46.

Figure 46: Peel off effect

Also, if the tensile failure is wanted to happen first, the compression layer should prevent a sudden compressive failure as the occurred in the first set of tests. In addition, the compressive layup also helped to delay shear, compression and crushing failure due to the stiffness brought around by the layers of IM7 and the force distribution characteristics of S-glass, both proving to be effective in compression applications.

The reason why achieving a failure initiated by tensile processes is that this is the most predictable failure mechanism in composite materials. Another important argument is that visual warnings of failure on the handlebar's layup had to be necessarily placed on top of it for the rider to notice.

Efforts were made with the loading nose and support designs to prevent the collapse and crushing of the tube. By increasing the surface area of them in contact with the bar, there is a greater spread in the load.

As the Figure 46 shows, when the graph of the Test 3 of the final tests reaches around 11.5 KN, the final failure occurs through shear. This happens towards the supports, a region where the layup also ends, as opposed to where the failure was occurring in the initial tests, which happened around the edge of the loading nose. The difference in material of these two regions, leads to a change in the curvature, shown in Figure 47. Shear failure might be promoted because of this reason.

Figure 47 and Figure 48 also show the reduction of the length of the span that had to be done. It also illustrates the fanning of the tensile side during the bending test, which is hugely important as it visually shows early damage to the material. In Figure 44 this is shown.

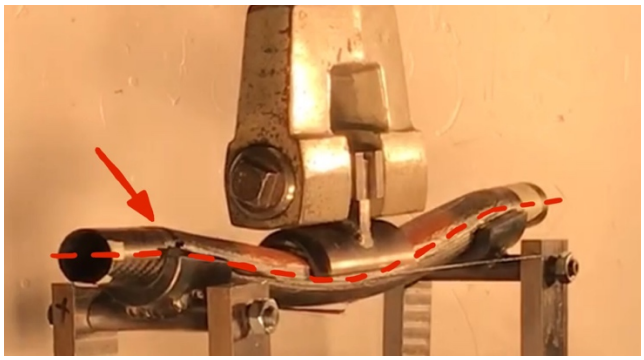

Figure 47: Bending shape Test 3 of final tests

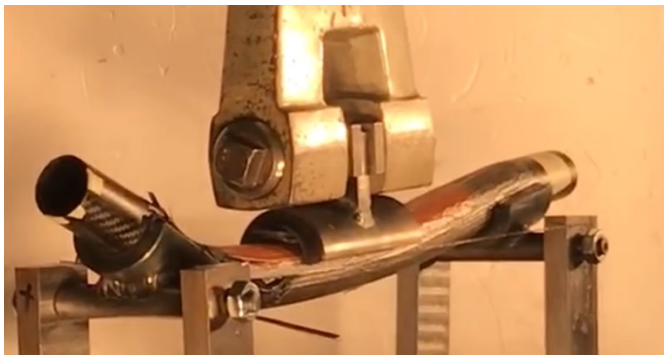

Figure 48: Failure in Test 3 of final tests

The results achieved met our aims and gave the desired pseudo-ductile behaviour set out for the project. However, there are areas that can be improved upon for future works. For future tests it would be advised that the layup is designed to extend along the tube, so that the supports within the bending test contact the layup. In the same way, the span needs to be increased. Also, as mentioned in the manufacturing section, efforts can be made to increase the surface quality by implementing an extra

film between the cotton layer and release film to prevent the cotton pattern being imprinted onto the layups surface. Besides, shear failure needs to be studied in detail in the simulation.

6. Conclusion

To conclude, a reinforced carbon fibre tube by means of a composite layup was made. Several layups were designed on FEA software using data from tests carried out on tubes without layups and then two best options were chosen, manufactured and applied to the tubes. These layups were later tested, and the results showed a pseudo-ductile behaviour. Consequently, a gradual failure of the composite layups was achieved, reaching in this way the aim of the project. What we have learnt on this project can be applied in future work to bicycle handlebars, making them safer.

7. References

[1] P. Norman, “Do carbon frames have a shelf life?,” 23 August 2016. [Online]. Available: https://www.cyclingweekly.com/news/latest-news/carbon-frames-shelf-life-277989.

[2] Z. Rácz and L. M. Vas, “Relationship between the flexural properties and,” 2005.

[3] M. Jalalvand, M. R.Wisnomb and G. Czélab, "Design and characterisation of advanced pseudo-ductile unidirectional thin-ply carbon/epoxy–glass/epoxy hybrid composites," 2016.

[4] G. Czél and M. R.Wisnom, "Demonstration of pseudo-ductility in high performance glass/epoxy composites by hybridisation with thin-ply carbon prepreg," 2013.

[5] M. Jalalvand, GergelyCzélab, T. Rev, M. Fotouhi, M. L.Longanab, O. J.Nixon-Pearsonb and M. R.Wisnomb, “Pseudo-ductility and reduced notch sensitivity in multi-directional all-carbon/epoxy thin-ply hybrid composites,” 2017.

[6] “Love HIGH SPEED,” [Online]. Available: http://www.lovehighspeed.com/lighting-for-high-speed/.

[7] “History of the Bicycle,” 2019. [Online]. Available: http://www.bicyclehistory.net/bicycle-history/history-of-bicycle/.

[8] “Bicycle handlebar,” [Online]. Available: https://en.wikipedia.org/wiki/Bicycle_handlebar#cite_note-1.

[9] J. Bracey, “Should you buy carbon handlebars over aluminium?,” 4 October 2016. [Online]. Available: https://www.cyclingweekly.com/news/product-news/buy-carbon-handlebars-aluminium-287138.

[10] “Difference Between Aluminum and Carbon Fiber,” [Online]. Available: http://www.differencebetween.net/object/difference-between-aluminum-and-carbon-fiber/.

Universidad de Oviedo

ESCUELA POLITÉCTINA DE INGENIERÍA DE GIJÓN

GRADO EN INGENIERÍA MECÁNICA

ÁREA DE INGENIERÍA DE MATERIALES

MANILLAR DE MATERIALES COMPUESTOS: TEST Y ANÁLISIS

D. César Martínez Fernández

TUTOR: D. MEISAM JALALVAND Y Dña. MARÍA JESÚS LAMELA REY

FECHA: MARZO 2019

Abstracto

Se realizaron ensayos en tubos de fibra de carbono con el objetivo de tener un buen entendimiento de cómo la fibra de carbono se comporta al ser sometida a una carga creciente hasta su rotura. Se pudo observar que todas las muestras rompieron de forma catastrófica y ningún aviso, ya fuese acústico o visual, pronosticó la inminente fractura del material. Estos datos fueron utilizados en estadios posteriores del proyecto para simular y luego aplicar una secuencia de capas de materiales compuestos sobre el tubo, como refuerzo, mostrando un fallo gradual antes de que la integridad estructural del tubo se vea comprometida. Con ello, se pretendía que el tubo en su conjunto presente cierta deformación visible antes de su rotura total. Finalmente, los tubos reforzados se rompieron en diversos ensayos y los resultados se compararon con aquellos obtenidos en los ensayos de los tubos sin refuerzo.

Índice de contenidos

1. Introducción

El manillar es el sistema de dirección de una bicicleta. El material más común utilizado en la fabricación de los manillares es el aluminio, gracias a su relativa ligereza con respecto al acero, y sus buenas propiedades mecánicas. No obstante, el énfasis de sacar al mercado bicicletas cada vez más ligeras, nuevos manillares de fibra de carbono comenzaron a introducirse en la industria. Éstos cuentan con mayor resistencia y menor densidad que los manillares de aluminio, propiedades clave en la mejora de las prestaciones de las bicicletas de competición. El uso de estos materiales posibilita además la fabricación de manillares con geometrías más complejas, adoptando perfiles aerodinámicos que reduzcan el drag.

La utilización de materiales compuestos en la fabricación de manillares de bicicleta confiere grandes ventajas, anteriormente expuestas. Sin embargo, estos materiales presentan una gran desventaja: son frágiles. Cuando la carga supera un cierto límite rompen de manera catastrófica, sin ningún tipo de deformación plástica que avise que la integridad estructural del manillar esté comprometida. Esta rotura súbita hace que muchos ciclistas de competición sean reacios a adoptar este tipo de manillares.

2. Objetivo y metodología

El objetivo de este trabajo es incrementar la seguridad de los manillares de bicicleta de fibra de carbono adhiriendo sobre ellos una secuencia de capas de distintos materiales compuestos. Con esto se pretende obtener un manillar de material híbrido que presente un comportamiento pseudodúctil en estadios de deformación previos a la rotura total del mismo, evitando así la fractura frágil.

En este contexto se adoptó un tubo de fibra de carbono, como modelo simplificado para utilizar como base en este proyecto. El trabajo fue dividido en cuatro secciones expuestas a continuación:

1. Tests iniciales.
2. Simulación con software de análisis de elementos finitos.
3. Fabricación.
4. Tests finales.

3. Trabajo realizado y resultados obtenidos

3.1. Tests iniciales

Por el simple acto de ir en bicicleta, el manillar se ve sometido a una serie de esfuerzos de flexión variables. Teniendo esto en cuenta, ensayos de fatiga podrían ser una opción válida. No obstante, debido al buen comportamiento a fatiga de la mayoría de los manillares fabricados con materiales compuestos de matriz polimérica, esta opción se acabó por descartar.

Otra opción que se consideró fue la de hacer ensayos de impacto, en los que se fijan pesos en ambos extremos del manillar y se deja caer desde cierta altura para analizar su comportamiento. Pese a la utilidad de la información que este enfoque podría proporcionar en el ámbito del fallo por impacto, este método no representa con precisión suficiente el punto de rotura, si se compara con el ensayo a flexión cuasi estático de 3 puntos. Es este lento desarrollo del ensayo de flexión lo que faculta el monitoreo de los distintos parámetros de interés. La disponibilidad de máquinas para ensayos de flexión, mordazas y anclajes hicieron que se adoptase este último método para este proyecto.

En un ensayo de flexión de tres puntos, las fibras en la parte superior del tubo están bajo compresión, y las fibras inferiores a tracción. Como predicción inicial, se asume que el tubo de fibra de carbono romperá antes por el lado de compresión, debido a que el comportamiento que este material presenta en este tipo de esfuerzos es, por regla general, peor que el mostrado bajo esfuerzos de tracción. Esto es debido a la configuración interna del material y se explica mediante un proceso denominado micro pandeo, por el que las fibras bajo esfuerzos de compresión se despegan de la matriz (por deformaciones elásticas o plásticas) y pandean.

El manillar está sometido a tres fuerzas: dos laterales aplicadas por las manos del ciclista en sentido descendente y la reacción transmitida por la potencia (parte que conecta el manillar con el resto de la bicicleta). En la *Ilustración 1* se recrea este escenario, pero adaptado al ensayo de flexión y siendo F una fuerza de magnitud arbitraria.

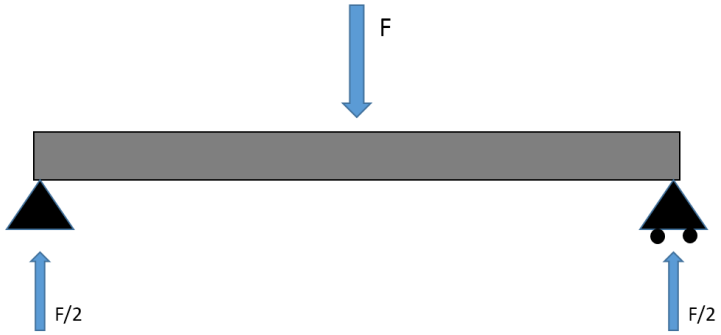

Ilustración 1. Representación de las caargas en un test de flexión.

En este proyecto se llevaron a cabo un total de tres ensayos sobre los tubos de fibra de carbono iniciales, compartiendo todos ellos las mismas dimensiones y propiedades. La velocidad de la nariz de carga se fijó a un valor constante, y de este modo valores de la fuerza de reacción sobre esta pieza se fueron midiendo para cada momento de tiempo.

3.1.1. Los tubos

Los valores dimensionales de los tubos sujetos a los ensayos se recogen en la *Tabla* 1.

Tabla 1. Dimensiones tubos.

Length (L)	500 mm
Outer diameter (OD)	30 mm
Inner diameter (ID)	28 mm
Thickness (T)	1 mm
Type of fibres	Woven

Un parámetro importante que considerar fue la relación de aspecto entre la distancia de separación entre los soportes y el diámetro exterior del tubo. Controlando que este valor no descendiese por debajo de 10 se evitaba un fallo iniciado por mecanismos de cortadura. Para el tubo seleccionado, tratando de acercarse lo más posible a las dimensiones de manillares comerciales, esta relación de aspecto fue igual a 15.

3.1.2. Condiciones de contorno

Para obtener flexión en el tubo se aplicaron las condiciones de contorno apropiadas. Siguiendo la configuración mostrada en la Ilustración 1, la rotación debe permitirse en ambos extremos del tubo. En cuanto a los desplazamientos, en uno de los lados se restringe el desplazamiento longitudinal, manteniendo el otro libre. El uso de goma en el montaje aseguró no sólo un correcto amarre del tubo con respecto a los soportes y nariz de carga, si no que también permitió cierto desplazamiento relativo entre las distintas partes, producto de las deformaciones sufridas por el tubo.

Los diseños de los soportes y la nariz de carga se vieron condicionados por las condiciones de contorno anteriores. Ambos soportes y la nariz presentan una sección de tubo longitudinal para incrementar la superficie de contacto con el tubo de fibra de carbono. El radio interior de estas regiones tubulares es de 17mm. Goma de 2mm de grosor se instaló para acomodar el espécimen en el montaje. Con esto se pretendía reducir los concentradores de esfuerzos en el tubo en las regiones de contacto, evitando así su fallo por aplastamiento. Los soportes laterales cuentan con un eje de sección variable alrededor del cual pivotan para acompañar el movimiento del tubo a medida que flexiona. Además, esta característica de su diseño aumenta la repetibilidad de los ensayos al facilitar el centrado del tubo en la máquina. En la *Ilustración 2* se muestra el montaje final con el tubo reposando sobre los soportes. Todo ello se une a la base del sistema de anclaje, la cual ya estaba fabricada.

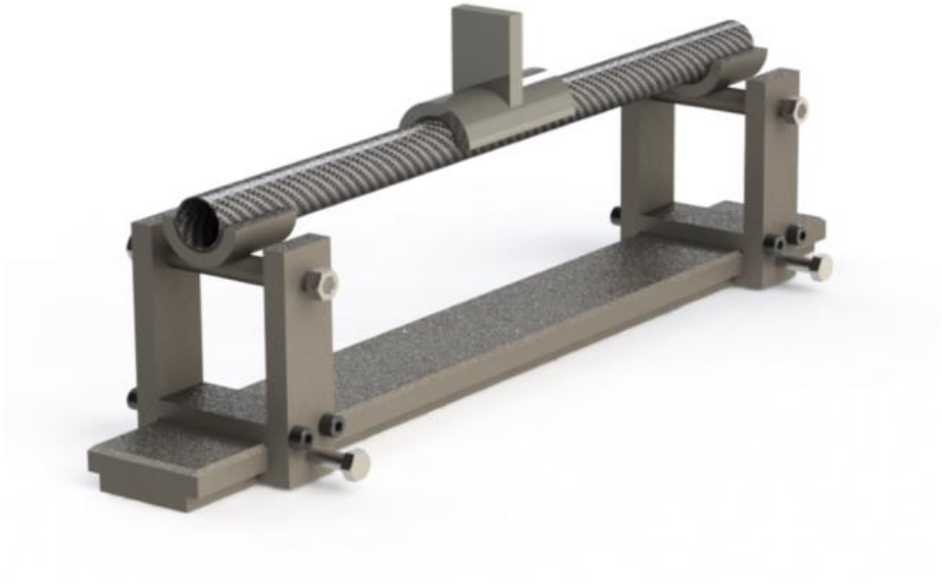

Ilustración 2. Montaje final

3.1.3. Medición

Se seleccionaron y aplicaron las galgas extensiométricas apropiadas en aquellos puntos de interés, donde era necesario conocer valores de las deformaciones. Siguiendo la teoría de flexión, el máximo momento flector, y en consecuencia la máxima tensión y deformación, se alcanzan en la sección transversal central del tubo, y va disminuyendo hasta llegar a cero en los extremos. En el primer ensayo se instaló una sola galga en la parte central del tubo en la zona de tracción.

Tras la realización de este primer test y una vez localizada la zona donde el tubo rompió, en los dos tubos restantes se aplicaron más galgas en las inmediaciones de esa zona, tanto en regiones de compresión como de tracción. Esto facilitó la adquisición de una distribución detallada de las deformaciones en las secciones de interés de los tubos. La recogida de datos se llevó a cabo con el software LabView.

3.1.4. Resultados y conclusiones

Las galgas extensiométricas miden la deformación en función del tiempo. En la *Ilustración 3* se recopilan las distintas posiciones de las galgas en cada uno de los tres ensayos iniciales y la deformación máxima medida en cada una de ellas antes de la rotura del espécimen. La línea roja evidencia la sección donde los tubos acabaron rompiendo (no se trata de una representación a escala).

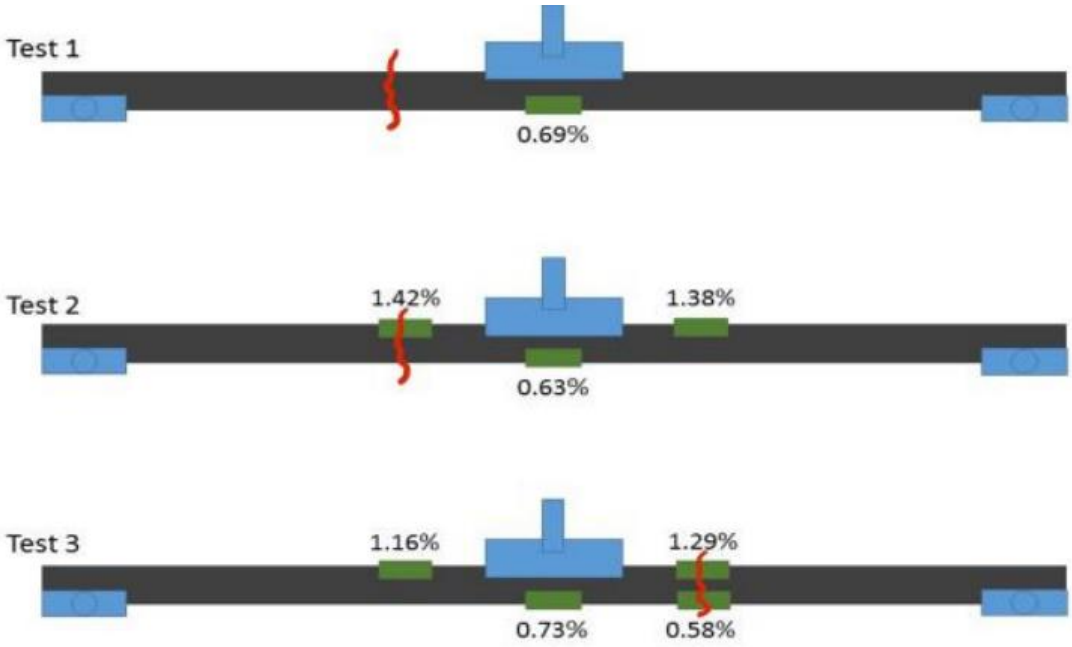

Ilustración 3. Deformaciones máximas medidas en los tests iniciales.

Las salidas de la máquina de ensayos son el desplazamiento de la nariz de carga y la fuerza aplicada, ambas por cada instante de tiempo transcurrido. En la *Gáfica 1* se muestra el comportamiento de los tres tubos sin refuerzo que se rompieron en los tests iniciales. La evolución de esta gráfica es casi lineal, evidenciando el modo de fallo frágil del material. La velocidad de avance en todos estos casos se mantuvo constante en 2mm/s.

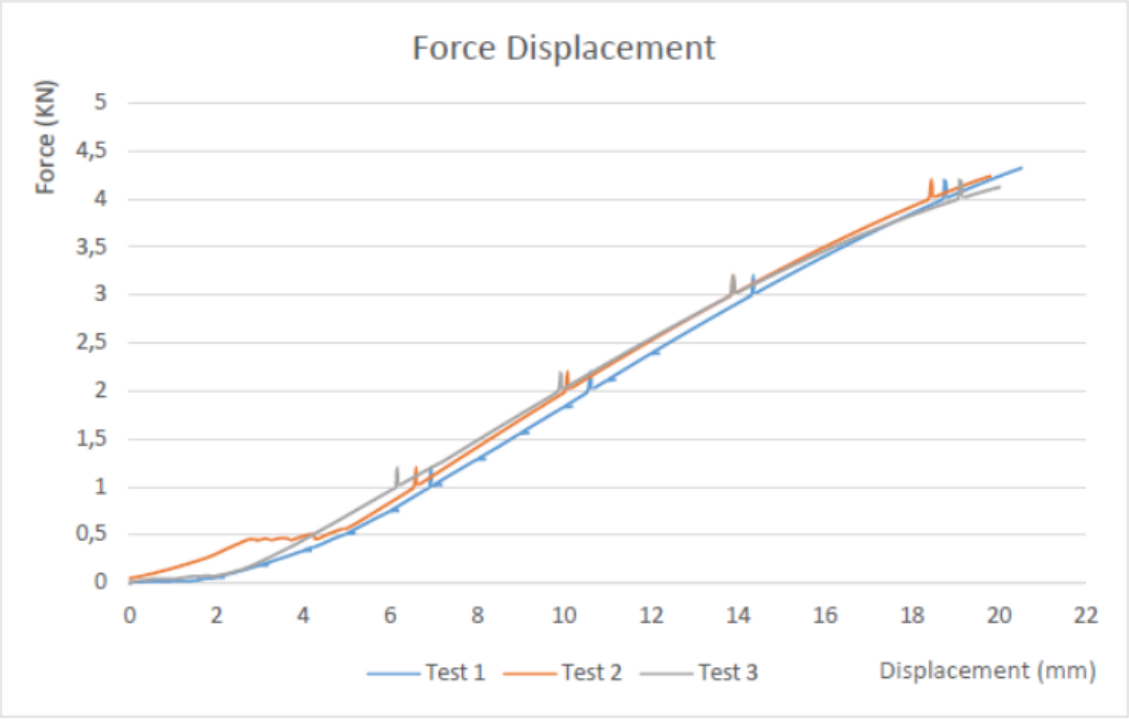

Gáfica 1. Fuerza-desplazamiento en los tests iniciales.

Los tubos, una vez la máquina ejercía una carga en torno a los 4,3kN, rompieron súbitamente, emitiendo un fuerte estallido. Además, ningún signo de deformación plástica fue aparente, una vez los fragmentos fueron observados. Además, atendiendo a los datos obtenidos de las galgas, se pudo demostrar que el fallo era iniciado en el lado de compresión ya que en esta zona las deformaciones eran mayores.

Una vez todos los datos y conclusiones de los ensayos iniciales sobre los tubos sin refuerzo fueron recopilados, se inició otra fase del proyecto: la de simulación.

3.2. Simulación

La fase de simulación tuvo como objetivo el diseño de un refuerzo que, una vez aplicado al tubo de fibra de carbono inicial, lograría conseguir un modelo de fallo similar a aquel encontrado en materiales dúctiles isotrópicos. Para hacer esto posible se utilizó el software de simulación ANSYS, específicamente su extensión para materiales compuestos.

Se importó un modelo del tubo realizado en SolidWorks como base para el posterior diseño de la secuencia de capas (o “layup”) que iban a constituir el refuerzo. A este modelo se le introdujeron las características del material apropiadas y se le aplicó la misma fuerza a la que rompieron los especímenes en los ensayos anteriores. Asimismo, se añadieron las mismas condiciones de contorno a las que estuvieron sometidos.

Una vez los valores de deformación en la simulación fueron lo suficientemente cercanos a aquellos alcanzados en los ensayos, fue el momento de comenzar con el diseño del refuerzo.

La primera cuestión que hubo que abordar fue que el inicio del fallo ocurría en las fibras sometidas a compresión. La intención era la de intentar retrasar lo más posible el fallo a compresión de forma que el tubo rompiese antes a tracción. El hecho de que los valores de resistencia última de las fibras vienen en términos de deformación a tracción, unido a lo impredecible del fallo a compresión en estos materiales, hicieron de ésta una estrategia válida que aplicar en este proyecto.

Después de probar diversos materiales de refuerzo en la simulación y estudiar la viabilidad de su adquisición, se acabaron eligiendo el IM7 y el YSH70, dos tipos de fibras de carbono unidireccionales y preimpregnadas. Estos dos materiales fueron los que mejor comportamiento mostraron en la simulación, produciendo el mecanismo de fallo requerido.

Para conseguir un fallo gradual del refuerzo que permita avisar al ciclista antes de que la integridad estructural del tubo se vea comprometida se colocaron las capas dce material como se muestra en la *Ilustración 4*. Las capas de S-Glass junto con las de IM7 en la parte superior (la sometida a compresión) tuvieron como objetivo no sólo rigidizar el tubo, si no que también distribuir los esfuerzos aplicados por la nariz de carga sobre una mayor superficie. De esta forma se reducieron los concentradores de esfuerzos en aquellas zonas de contacto del tubo con ambos extremos de la nariz.

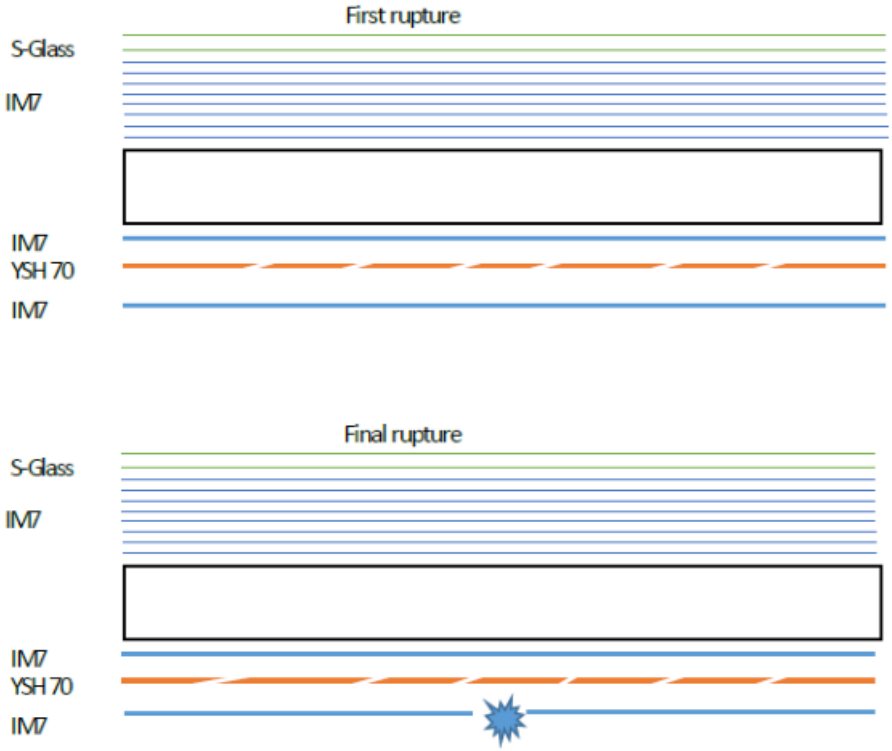

Ilustración 4. Modo de fallo "layup"

En la parte a tracción se intercalaron capas de IM7 y YSH70 que, por sus distintos límites de rotura, se pretendía lograr la fractura de las capas de YSH 70 mientras que la exterior de IM7 se mantenía aparentemente intacta. Con un progresivo incremento de la carga sucesivos fallos en las capas de YSH 70 iban dañando la capa exterior y reduciendo la sección del espécimen, haciendo que llegase un punto en el cual el refuerzo no podía soportar más carga y colapsaba produciendo un “efecto de abanico”.

3.3. Fabricación

La elaboración del refuerzo se acometió sobre el mismo tubo de fibra de carbono, mediante un método de fabricación conocido como “vacuum forming”. A raíz de las simulaciones se optó por fabricar dos refuerzos. Ambos compartían los mismos materiales, pero se varió la secuencia de capas utilizadas.

Layup 1

- Compressive/top side of bar	→	3 S-Glass Layers
	→	10 IM7 Layers
-Tensile/bottom side of bar	→	2 IM7 Layers
	→	1 YSH70 Layer

Layup 2

- Compressive/top side of bar	→	3 S-Glass Layers
	→	14 IM7 Layers
-Tensile/bottom side of bar	→	2 IM7 Layers
	→	2 YSH70 Layers

Inicialmente, las capas de los materiales se midieron y fueron cortadas a la longitud requerida. Acto seguido, se procedió al pegado de éstas sobre el tubo, procurando su correcta alineación. Una vez las capas se encontraban fijadas en la posición deseada, el conjunto se envolvió en una serie de materiales con los que se conseguiría un sello estanco, tal y como muestra la *Ilustración 5*. Después de la instalación de una válvula, se procedió a introducir la muestra en la autoclave, un horno capaz de calentar a temperaturas suficientes para el curado de las resinas de las capas de material preimpregnado. El autoclave aplica durante el proceso de curado presión, lo que permite que la adhesión sea satisfactoria. Para prevenir burbujas de aire en el interior de la bolsa se conectó una vía que aplicaba vacío durante el proceso.

Ilustración 5. Sellado del conjunto

Una vez el ciclo de curado hubo finalizado se procedió a la retirada de los materiales anteriormente citados y se midió el peso de los nuevos tubos reforzados. En la *Tabla 2* se comparan los pesos de los dos tubos con los dos tipos de refuerzos con el del tubo original.

Tabla 2. Peso del tubo antes y después de aplicar los refuerzos

	Tubo original	Tubo reforzado 1	Tubo reforzado 2
Peso (g)	68	116	132
Incremento (%)	-	70	90

3.4. Tests finales

Los tubos reforzados, una vez hubo concluido su fabricación, se ensayaron en la máquina utilizada en los tests iniciales. Se mantuvo la distancia de separación entre apoyos y la velocidad de avance.

3.4.1. Layup 1

Test 1

En este ensayo el tubo rompió alcanzados los 7500N. En la *Gáfica 2* se puede observar una curvatura con tendencia a la horizontal en los últimos valores de desplazamientos. Esto evidencia la labor que realiza el refuerzo. La rotura gradual de las fibras de éste, genera el comportamiento pseudo-plástico del material. No obstante, debido a su prematuro fallo en uno de los extremos del tubo provocado por mecanismos de cortadura, el resultado de este ensayo no fue del todo satisfactorio.

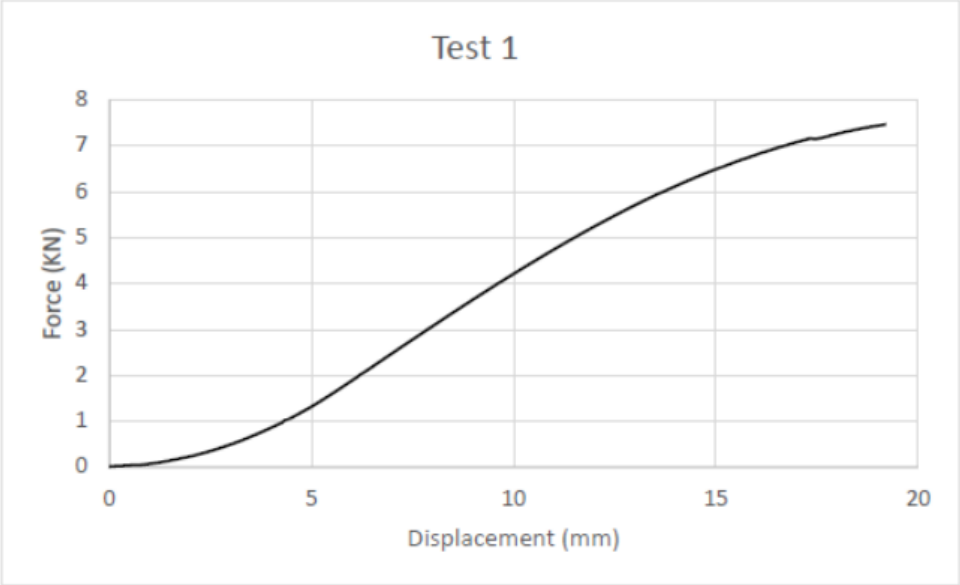

Gáfica 2. Fuerza-desplazamiento Test 1.

En la *Ilustración 6* se muestra el modo de fallo a cortadura del primer test. La rotura se originó en la zona donde terminaba el refuerzo. El concentrador de tensiones generado, unido al ejercido por los apoyos en la misma zona, acabó por debilitar el tubo antes de que el refuerzo hubiese realizado su función correctamente.

Ilustración 6. Zona afectada Test 1.

Test 2

En el segundo ensayo se utilizó el mismo modelo de refuerzo. Con lo aprendido en el ensayo anterior se redujo la distancia de separación entre los apoyos, tal y como se muestra en la *Ilustración 7*. De esta forma se reducían los concentradores de esfuerzos en esa zona problemática sin refuerzo, pero, como contrapartida, se corría el riesgo de que la reducción de la relación de aspecto entre el diámetro del espécimen y la separación entre apoyos diera otros problemas. No obstante, se consideró que era un riesgo asumible para el correcto desarrollo del proyecto y se acometió el ensayo.

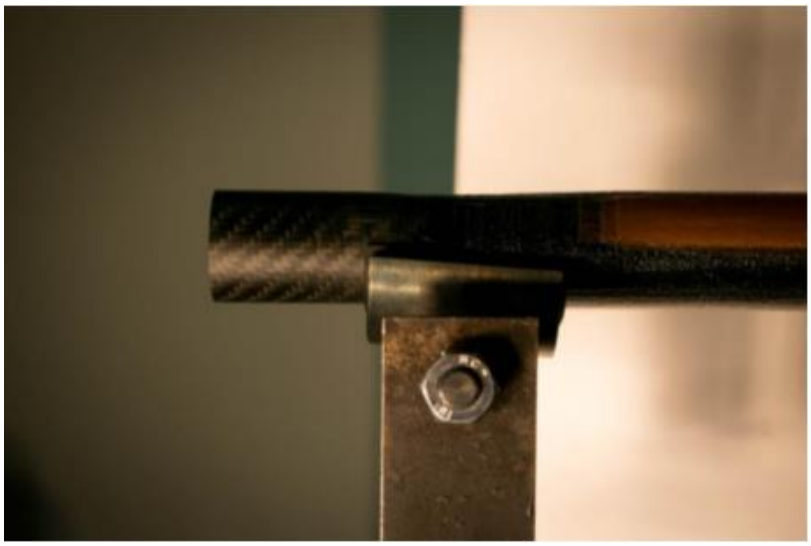

Ilustración 7. Configuración de los apoyos en el Test 2.

En la *Gáfica 3* la curva fuerza-desplazamiento muestra el comportamiento esperado del refuerzo. La rotura de las distintas capas de material se traduce en esta evolución no lineal, con saltos en distintos instantes de desplazamiento. Llegados a este punto uno de los dos objetivos fue alcanzado: el refuerzo rigidizó el tubo, haciendo que el conjunto soportase unos valores de carga de en torno a los 10 KN y cierto comportamiento propio de materiales plásticos fue alcanzado. Sin embargo, el "efecto de abanico" pronosticado en la fase de simulación no fue percibido, un aspecto considerado necesario para identificar con facilidad por parte del ciclista de que el manillar estaba sufriendo daños.

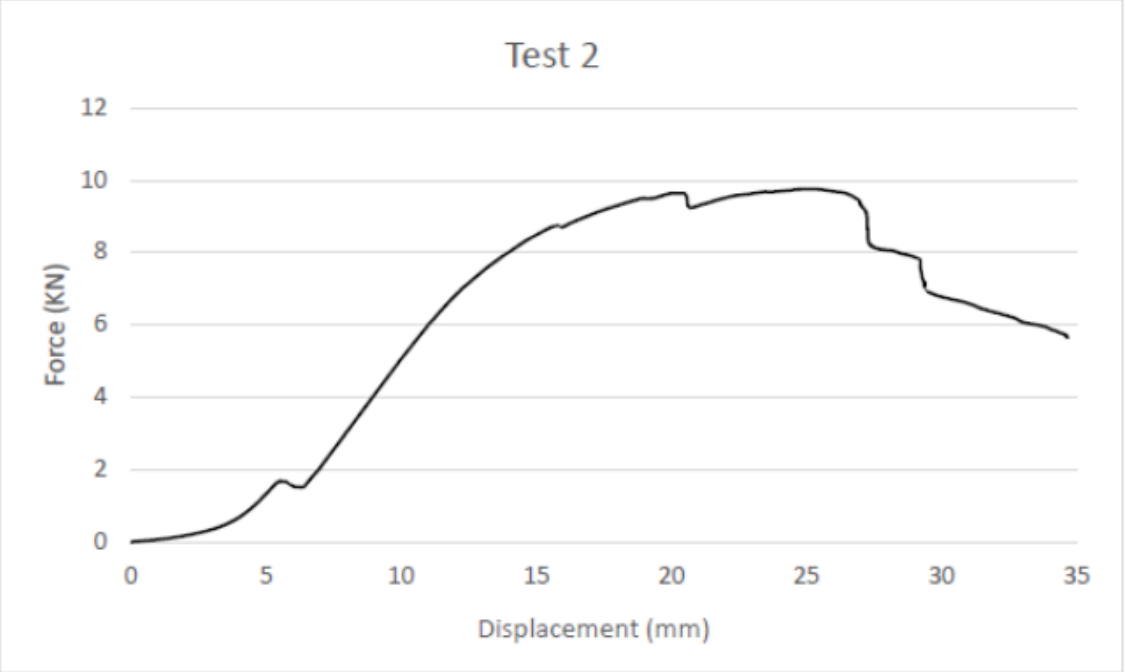

Gáfica 3. Fuerza-desplazamiento Test 2.

3.4.2. Layup 2

Test 3

En el tercer y último ensayo se utilizó el espécimen con el segundo modelo de refuerzo. En este caso, al contar con mayor número de capas en el refuerzo, se alcanzaron los 11000N antes del fallo final. En la *Gáfica 4* la curva fuerza-desplazamiento muestra un evidente comportamiento pseudo-plástico, propio de materiales dúctiles isotrópicos como el aluminio, entre otros. Dos zonas bien diferenciadas: una elástica con una evolución lineal hasta los 6,5 kN y, a partir de ahí, una zona plástica producto de las sucesivas roturas del material explicadas anteriormente.

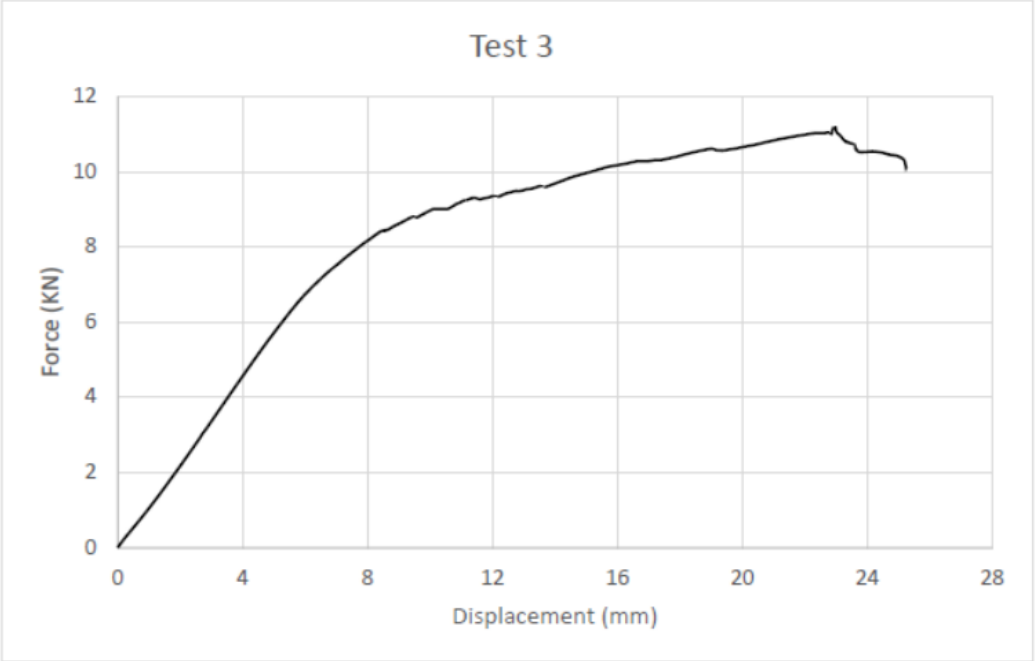

Gáfica 4. Fuerza-desplazamiento Test 3

En el transcurso del ensayo se pudieron apreciar una serie de señales visuales y acústicas que apuntaban al fallo gradual del refuerzo, hasta que en las fases finales del mismo se desprendió una lámina como la que aparece en la *Ilustración 8.*

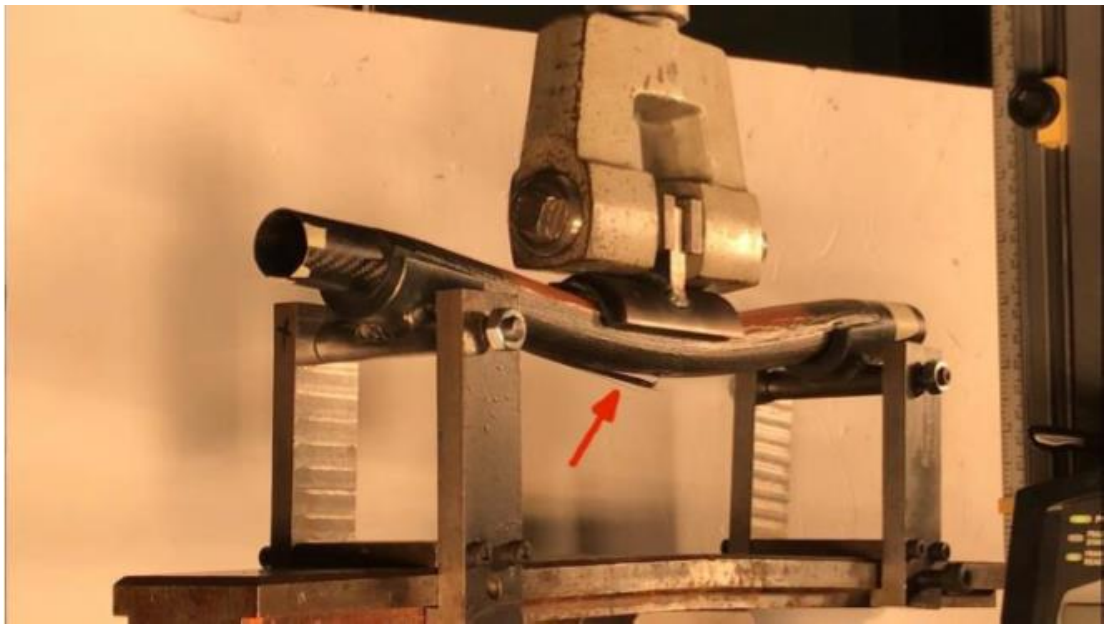

Ilustración 8. Fallo gradual en el Test 3

4. Conclusiones

Los resultados obtenidos en los ensayos iniciales y finales fueron analizados y comparados.

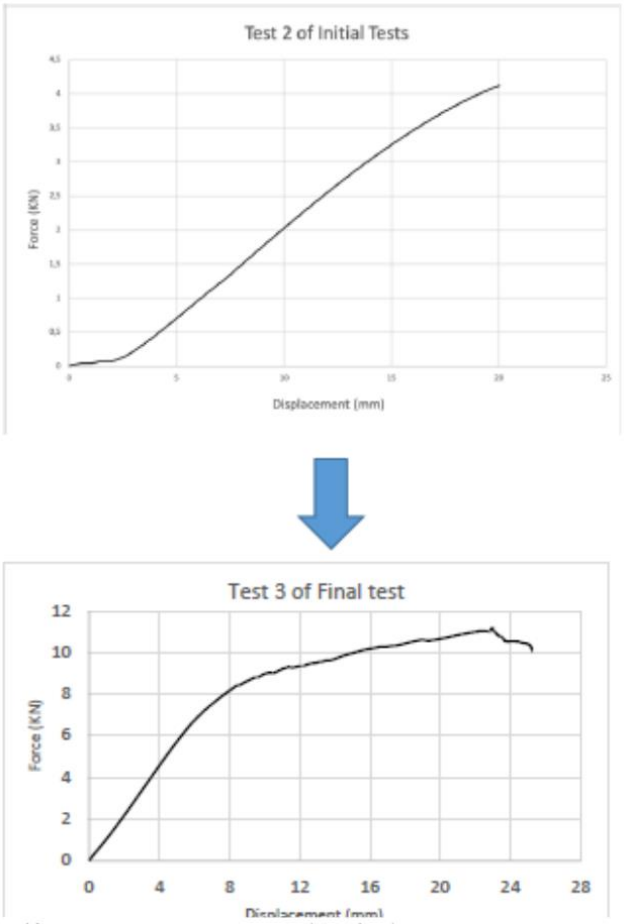

Este proyecto se inició con un tubo de fibra de carbono que presentaba un comportamiento frágil. La carga aplicada iba aumentando proporcionalmente hasta que el punto límite de rotura del material llega y el fallo ocurre de forma repentina y catastrófica. En la gráfica inferior, con el diseño, elección y configuración de las distintas capas de refuerzo que se le aplicaron al anterior tubo, se logró un comportamiento pseudo-plástico. Presenta zonas que son claramente apreciables. Una evolución elástica en las primeras fases del ensayo, pasando por una zona de transición, para finalmente simular una deformación plástica propia de materiales dúctiles hasta que el material rompe. Sonidos y avisos visuales estuvieron presentes durante los ensayos provocados por la rotura de las fibras del refuerzo que lograron el buscado “efecto de abanico” mencionado.

Estos resultados hicieron que los objetivos iniciales fuesen cumplidos. Un estudio más pormenorizado del refuerzo obtenido podría ser de gran ayuda para iteraciones futuras, realizando otros tipos de tests, como el de fatiga o el de impacto. Finalmente, este concepto se podrá aplicar a manillares de bicicleta comerciales para incrementar la seguridad de los ciclistas en las carreteras.